

1 **Exploring the drivers of the increased ozone production in Beijing in**
2 **summertime during 2005-2016**

3 Wenjie Wang¹, David D. Parrish², Xin Li^{1,3,4} *, Min Shao^{2,1}, Ying Liu¹, Ziwei Mo²,
4 Sihua Lu¹, Min Hu¹, Xin Fang¹, Yusheng Wu^{1,#}, Limin Zeng¹, Yuanhang Zhang¹

5
6
7 ¹ State Key Joint Laboratory of Environmental Simulation and Pollution Control,
8 College of Environmental Sciences and Engineering, Peking University, Beijing,
9 China

10 ² Institute for Environmental and Climate Research, Jinan University,
11 Guangzhou 511443, China

12 ³ International Joint Laboratory for Regional Pollution Control, Ministry of
13 Education, Beijing, 100816, China

14 ⁴ Collaborative Innovation Centre of Atmospheric Environment and Equipment
15 Technology, Nanjing University of Information Science & Technology, Nanjing,
16 210044, China

17 [#] now at Department of Physics, University of Helsinki, Helsinki, Finland

18
19
20
21
22 * Corresponding author.

23 Address: College of Environmental Sciences and Engineering, Peking
24 University, Beijing 100871, China

25 Phone: 86-10-62757973

26 Email: li_xin@pku.edu.cn

27

28 **Abstract**

29 In the past decade, average PM_{2.5} concentrations decreased rapidly under the
30 strong pollution control measures in major cities in China; however, ozone (O₃)
31 pollution emerged as a significant problem. Here we examine a unique (for China) 12-
32 year data set of ground-level O₃ and precursor concentrations collected at an urban site
33 in Beijing (PKUERS), where the maximum daily 8 h average (MDA8) O₃ concentration
34 and daytime Ox (O₃ + NO₂) concentration in August increased by 2.3 ± 1.2 ppbv ($+3.3$
35 $\pm 1.8\%$) yr⁻¹ and 1.4 ± 0.6 ($+1.9 \pm 0.8\%$) yr⁻¹ respectively from 2005 to 2016. In contrast,
36 daytime concentrations of nitrogen oxides (NO_x) and the OH reactivity of volatile
37 organic compounds (VOCs) both decreased significantly. Over this same time, the
38 decrease of particulate matter, and thus the aerosol optical depth, led to enhanced solar
39 radiation and photolysis frequencies, with near-surface $j(\text{NO}_2)$ increasing at a rate of
40 $3.6 \pm 0.8\%$ yr⁻¹. We use an observation based box model to analyze the combined effect
41 of solar radiation and ozone precursor changes on ozone production rate, P(O₃). The
42 results indicate that the ratio of the rates of decrease of VOCs and NO_x (about 1.1) is
43 inefficient in reducing ozone production in Beijing. P(O₃) increased during the decade
44 due to more rapid atmospheric oxidation caused to a large extent by the decrease of
45 particulate matter. This elevated ozone production was driven primarily by increased
46 actinic flux due to PM_{2.5} decrease and to a lesser extent by reduced heterogeneous
47 uptake of HO₂. Therefore, the influence of PM_{2.5} on actinic flux and thus on the rate of
48 oxidation of VOCs and NO_x to ozone and to secondary aerosol (i.e., the major
49 contributor to PM_{2.5}) is important for determining the atmospheric effects of controlling
50 the emissions of the common precursors of PM_{2.5} and ozone when attempting to control
51 these two important air pollutants.

52

53

54

55 **1 Introduction**

56 Tropospheric ozone (O_3) plays a key role in the oxidizing capacity of the
57 atmosphere and affects the global climate; high concentrations of ground-level ozone
58 are harmful to human health and ecosystems (Monks et al., 2015;Fiore et al., 2009).
59 Ozone is produced rapidly in sun-lit polluted air by photochemical oxidation of
60 volatile organic compounds (VOCs) in the presence of nitrogen oxides ($NO_x \equiv NO +$
61 NO_2) (Atkinson, 2000). In recent years, China has undergone rapid economic
62 development, resulting in higher demand for energy, and greater usage of fossil fuels.
63 As a result, high emissions to the atmosphere produce heavy pollution in eastern
64 China, which now suffers from severe ozone pollution, especially in urban areas,
65 where the daily maximum 8 h average (MDA8) ozone level often exceeds the
66 standard of 80 ppb (Jinfeng et al., 2014;Wang et al., 2011;Zhang et al., 2014;Lu et al.,
67 2018;Li et al., 2019b). A recent study reported that the national warm-season
68 (April–September) fourth highest MDA8 ozone level (86.0 ppb) and the number of
69 days with MDA8 values of > 70 ppb was much higher than regional averages in
70 Japan, South Korea, Europe, or the United States (Lu et al., 2018). Satellite
71 observations found that regional ozone concentrations in eastern China increased by
72 7% between 2005 and 2010 (Verstraeten et al., 2015). From 2013 to 2017, the O_3
73 concentrations in 74 cities as a whole showed an upward trend with Beijing-Tianjin-
74 Hebei region being the most serious (Li et al., 2019b;Lu et al., 2018). Better
75 understanding of the causes of elevated ozone in China is important for developing
76 effective emission control strategies to reduce the ozone pollution problem.

77 Aerosols impact ozone production primarily in two ways: alteration of photolysis
78 rates by aerosol radiative influence and heterogeneous reactions occurring on the
79 aerosol surface. The reduction of photolysis frequencies by the extinction effect of
80 aerosol and thus its influence on ozone production has been explored in the past
81 (Dickerson et al., 1997;Castro et al., 2001;Real and Sartelet, 2011;Gerasopoulos et al.,
82 2012;Wang et al., 2019). Absorbing aerosols reduce photolysis frequencies

83 throughout the boundary layer, and as a result decrease near-surface photochemical
84 ozone production (de Miranda et al., 2005; Jacobson, 1998; Wendisch et al., 1996; Raga
85 et al., 2001). Conversely, scattering aerosols in the boundary layer increase photolysis
86 frequencies throughout the troposphere, and thereby increase ozone production aloft
87 (Jacobson, 1998; Tian et al., 2019; Dickerson et al., 1997). The importance of aerosol
88 heterogeneous reactions in ozone photochemistry in China has been previously
89 investigated in model studies (Lou et al., 2014; Li et al., 2018b; Xu et al., 2012; Li et
90 al., 2019b). The effects of NO₂, NO₃, and N₂O₅ heterogeneous reactions showed
91 opposite O₃ concentration changes in VOC-limited and NO_x-limited regions. In a
92 VOC-limited region, NO₂, NO₃, and N₂O₅ heterogeneous reactions lead to ozone
93 concentration increases (Lou et al., 2014; Xu et al., 2012). The heterogeneous reaction
94 of HO₂ decreases ozone production in both VOC-limited and NO_x-limited regions by
95 decreasing the reaction rate of HO₂ with NO (Lou et al., 2014; Li et al., 2019b).

96 In the past decade, Eastern China has experienced severe fine particulate matter
97 (PM_{2.5}) pollution in winter (Zhang et al., 2016), and this issue has been the main focus
98 of the government's air pollution control strategy. These stringent emission control
99 measures have significantly decreased the concentrations of particulate matter in many
100 Chinese cities. During 2008-2013, ground-level PM_{2.5} estimated from satellite-
101 retrieved aerosol optical depth (AOD) in China declined at a rate of 0.46 μg m⁻³ year⁻¹
102 (Ma et al., 2016b). Another study indicated that the annual average concentration of
103 PM_{2.5} in Beijing decreased by 1.5 μg m⁻³ year⁻¹ and 27% in total from 2000 to 2015
104 under the implementation of 16 phases' air pollution control measures (Lang et al.,
105 2017). Hu et al (2017) reported that PM_{2.5} in Beijing declined significantly from 2006
106 to 2016, and meanwhile solar radiation increased (Hu et al., 2017). However, despite
107 the reduction in emissions of particulate matter (PM) and ozone precursors, ozone
108 concentrations increased, even while PM concentrations decreased.

109 In Beijing, the second largest city in China, with rapid economic development and
110 urbanization in recent years, ozone pollution is one of the worst among China's cities.
111 Thus, Beijing is a representative city in which to study urban ozone pollution in China.

112 Despite extensive study of the relationship between ozone and its precursors in Beijing
113 and other mega cities in China (Zhang et al., 2014;Chou et al., 2011;Lu et al., 2019;Liu
114 et al., 2012), there remains a lack of understanding of the cause of the long-term surface
115 ozone concentration increase that accompanied reductions in precursor emissions. In
116 this study, we utilize measurements from a representative urban site in Beijing to
117 explore how the variations in solar radiation and heterogeneous reactions influence the
118 trend of ozone and the coupling effect of aerosol and ozone precursor changes on ozone
119 production. Our overall goal is to determine the extent to which increasing actinic flux
120 caused by the decline in PM contributed to the observed increase in ozone
121 concentrations. This research provides a clearer understanding of how efforts to reduce
122 PM concentrations affect ozone concentrations, and thus informs air quality
123 improvement efforts in China's urban areas.

124 **2 Materials and methods**

125 **2.1 Measurements of air pollutants, photolysis frequencies and aerosol surface** 126 **concentration**

127 Ambient air pollutants and photolysis frequencies were measured at an urban site
128 in Beijing in August between 2005 and 2016. The site (39.99° N, 116.31°E) was located
129 on the roof of a six story building (~20m above the ground level) on the campus of
130 Peking University (PKUERS) near the 4th Ring Road with high density of traffic, but
131 without obvious industrial or agricultural sources (Wehner et al., 2008). Temporal
132 trends of air pollutants and composition of VOCs are thought to be representative for
133 the whole of Beijing (Wang et al., 2010;Xu et al., 2011;Zhang et al., 2012). Measured
134 parameters include O₃, NO_x, CO, SO₂, C₂ - C₁₀ VOCs, photolysis frequencies and
135 aerosol surface concentration. The measurement techniques are included in the Table 1.

136 During 2006 and 2008, ambient levels of VOCs were measured using an online
137 GC-FID system built by the Research Center for Environmental Changes (RCEC;
138 Taiwan). A detailed description of this system and QA/QC procedures can be found in

139 Wang et al. (Wang et al., 2004). During August 2007 and 2009, ambient VOCs were
140 measured using a commercial GC-FID/PID system (Syntech Spectra GC955 series
141 600/800 analyzer) (Xie et al., 2008;Zhang et al., 2014). From 2010 to 2016, VOCs were
142 measured using a cryogen-free online GC-MS/FID system developed by Peking
143 University. A detailed description of this system and QA/QC procedures can be found
144 in Yuan et al. and Wang et al. (Yuan et al., 2012;Wang et al., 2014). Formaldehyde
145 (HCHO) concentrations were measured by a Hantzsch fluorimetry.

146 Photolysis frequencies (including $j(\text{O}^1\text{D})$, $j(\text{NO}_2)$, $j(\text{HONO})$, $j(\text{HCHO})_M$,
147 $j(\text{HCHO})_R$, $j(\text{H}_2\text{O}_2)$) were calculated from solar actinic flux spectra measured by a
148 spectroradiometer as described by Bohn et al. (Bohn et al., 2008). The particle number
149 size distributions were measured by a system consisting of a Nano-SMPS (TSI
150 DMA3085 + CPC3776) and a SMPS (TSI DMA3081 + CPC3775). Aerosol surface
151 concentration (Sa) during 2006-2016 was calculated from the measured particle number
152 size distributions between 3 nm and 700 nm by assuming the particles are spherical in
153 shape.

154 **2.2 Estimate of photolysis frequencies**

155 Photolysis frequencies were measured in August 2011-2014 and 2016. The
156 Tropospheric Ultraviolet and Visible (TUV) radiation model (version 5.3) was used to
157 calculate photolysis frequencies in August over the entire 2006-2016 period under
158 clear-sky conditions. TUV uses the discrete-ordinate algorithm (DISORT) with four
159 streams and calculates the actinic flux spectra with a wavelength range of 280 – 420 nm
160 in 1 nm steps and resolution. We used observed aerosol optical properties including
161 AOD, single scattering albedo (SSA) and Ångström exponent (AE), total ozone column
162 to constrain the TUV model (Madronich, 1993). The calculated values agree well with
163 measured results as shown in Figure 1 indicating that the TUV model accurately
164 calculated the photolysis frequencies. Data of photolysis frequencies under cloudless
165 conditions were selected according to the presence of AOD data since AOD
166 measurements were not possible under cloudy conditions.

167 **2.3 Measurements of aerosol optical properties**

168 Aerosol optical properties were measured with a CIMEL Sun photometer
169 (AERONET level 1.5 and level 2.0 data collection, <http://aeronet.gsfc.nasa.gov/>) at the
170 Beijing-CAMS site (39.933°N, 116.317°E) and at the Beijing site (39.977N,116.381E).
171 The instrumentation, data acquisition, retrieval algorithms and calibration procedure,
172 which conform to the standards of the AERONET global network, are described in
173 detail by Fottiadi et al. (Fottiadi et al., 2006). The solar extinction measurements taken
174 every 3 minutes within the spectral range 340 – 1020 nm were used to compute AOD
175 at 340, 380, 440, 500, 675, 870, 970 and 1020 nm. The overall uncertainty in AOD data
176 under cloud-free conditions was 0.02 at a wavelength of 440 nm (Dubovik and King,
177 2000). In this study, AOD at the wavelength of 380nm was chosen for analysis. This
178 wavelength was selected as it is more representative of $j(\text{NO}_2)$. In addition to AOD, that
179 network also provided single scattering albedo (SSA) and Ångström exponent (AE)
180 data.

181 Cloud optical thickness (COT) was acquired from Aura satellite measurements
182 with a time resolution of 24 hours. Total ozone column was obtained by OMI (Ozone
183 Monitoring Instrument), using overpass data.

184 **2.4 Trend analysis method**

185 A simple linear regression (the least-squares method) was implemented to
186 investigate temporal trends of ozone, precursors, aerosol optical properties, $\text{PM}_{2.5}$ and
187 photolysis frequencies. The null hypothesis is that air pollutants and time have no
188 linear relationship and this was tested using the standard F-statistic test (ratio of the
189 mean-square regression to the mean-square residual). The p value associated with the
190 F-statistic is the probability of mistakenly rejecting the null hypothesis (** $p < 0.01$; *
191 $p < 0.05$). The p values for the trends of different parameters are summarized in Table
192 2.

193 **2.5 Chemical box model**

194 Ozone production rate, $P(O_3)$, is calculated by a chemical box model. This model
 195 is based on the compact Regional Atmospheric Chemical Mechanism version 2
 196 (RACM) described by Goliff et al. (Goliff et al., 2013), which includes 17 stable
 197 inorganic species, 4 inorganic intermediates, 55 stable organic compounds and 43
 198 intermediate organic compounds. Compounds that are not explicitly treated in the
 199 RACM are lumped into species with similar functional groups. The isoprene
 200 mechanism includes a more detailed mechanism based on the Leuven Isoprene
 201 Mechanism (LIM) proposed by Peeters et al. (Peeters et al., 2009). A detailed
 202 description of this model can be found in Tan et al. (Tan et al., 2017).

203 In this study, the model was constrained by measured hourly average CO, NO₂,
 204 O₃, SO₂, NMHCs (56 species), HCHO, photolysis frequencies, temperature, pressure,
 205 and relative humidity. HONO was not measured. HONO concentrations are generally
 206 underestimated by the gas phase reaction source of HONO (OH + NO → HONO) in
 207 urban areas due to the emission of HONO and the heterogeneous reaction of NO_x at
 208 surfaces to form HONO, both of which are related to NO_x concentration. As a result,
 209 the HONO concentration was calculated according to the concentration of NO₂ and
 210 the observed ratio of HONO to NO₂ at an urban site in Beijing, which had a marked
 211 diurnal cycle (Hendrick et al., 2014). For the model calculation, the ratio of HONO to
 212 NO₂ is equal to 0.08 at 6:00 and decreases linearly from 0.08 to 0.01 during 6:00 -
 213 10:00 reflecting increasing photolysis of HONO, and maintains the value of 0.01
 214 during 10:00-18:00. In this study, we focused on daytime $P(O_3)$ (6:00 - 18:00), thus
 215 the nocturnal HONO concentrations were not required.

216 RO₂, HO₂, OH were simulated by the box model to calculate the ozone
 217 production and loss rates as shown in Equations E1 and E2 as derived by Mihelcic et
 218 al. (Mihelcic et al., 2003).

$$219 \quad P(O_3) = k_{HO_2+NO} [HO_2][NO] + \sum (k^i_{RO_2+NO} [RO_2^i][NO]) - k_{OH+NO_2} [OH][NO_2] - L(O_3) \quad E1$$

$$220 \quad L(O_3) = (\theta j(O^1D) + k_{OH+O_3} [OH] + k_{HO_2+O_3} [HO_2] + \sum (k^j_{alkene+O_3} [alkene^j])) [O_3] \quad E2$$

221 where θ is the fraction of O¹D from ozone photolysis that reacts with water vapor. i and
222 j represent the number of species of RO₂ and alkenes, respectively.

223 The model runs were performed in a time-dependent mode with two days' spin-
224 up. A 24 h lifetime was introduced for all simulated species, such as secondary species
225 and radicals, to approximately simulate dry deposition and other losses of these
226 species (Lu et al., 2013). This lifetime corresponds to an assumed deposition velocity
227 of 1.2 cm s⁻¹ and a well-mixed boundary layer height of about 1 km. Sensitivity tests
228 show that this assumed deposition lifetime has a relatively small influence on the
229 reactivity of modeled oxidation products and RO_x radicals.

230 Aerosols can influence O₃ production by heterogeneous reactions such as uptake
231 of HO₂, NO₂, N₂O₅ and NO₃. For these species, the heterogeneous uptake of HO₂ is
232 expected to have the largest effect on rapid ozone production in summertime and VOC-
233 limited conditions (Li et al., 2019b). Thus, the effect of heterogeneous reaction of HO₂
234 on ozone production was simulated in the chemical box model using RH corrected
235 aerosol surface concentration (S_{aw}) and uptake coefficient of HO₂. The rate of change
236 in HO₂ due to irreversible uptake is expressed by E3.

$$237 \quad \frac{dC}{dt} = \frac{\gamma_{HO_2} \times S_{aw} \times v \times C}{4} \quad E3$$

238 Where C , v , and γ_{HO_2} are the gas phase concentration, mean molecular velocity, and
239 uptake coefficient, respectively. To derive S_{aw} we used the measured hygroscopic
240 factor (Liu et al., 2009) and measured RH to correct the measurement-derived S_a to
241 ambient conditions. In this study, we chose $\gamma_{HO_2} = 0.2$ provided by laboratory
242 measurements of HO₂ uptake by aerosol particles collected at two mountain sites in
243 eastern China (Taketani et al., 2012). The effects of HO₂ uptake on P(O₃) in Beijing in
244 2006 were simulated assuming that the product of HO₂ uptake by aerosols is either
245 H₂O or H₂O₂. The results indicate that the two scenarios showed no significant
246 difference because the recycling of HO_x radicals from H₂O₂ is inefficient (Li et al.,
247 2019b). In the following simulations in this study, the product of HO₂ uptake by
248 aerosols is taken to be H₂O.

249 Heterogeneous uptake of N₂O₅, NO₂ and NO₃ was included in the chemical box

250 model. This includes $\gamma_{\text{N}_2\text{O}_5} = 0.007$ for converting N_2O_5 to HNO_3 (Wang et al., 2017),
251 $\gamma_{\text{NO}_2} = 1 \times 10^{-5}$ for conversion of NO_2 to HONO and HNO_3 (which yields a good
252 simulation of HONO/ NO_2 concentration ratios in China (Shah et al., 2020)) and γ_{NO_3}
253 $= 1 \times 10^{-3}$ for conversion of NO_3 to HNO_3 (Jacob, 2000).

254 **3 Results and discussion**

255 **3.1 Trend of ozone**

256 Ozone pollution levels can be characterized by a number of metrics. Table 3 lists
257 10 ozone metrics and their definition summarized by Lu et al. (2018). We classify these
258 indicators into four categories: (1) metrics that characterize general levels of ozone:
259 median value of hourly ozone concentrations (median), daily maximum 8 h average
260 ozone concentration (MDA8) and daytime average ozone concentration (DTAvg); (2)
261 metrics that characterize extreme levels of ozone: daily maximum 1 h average ozone
262 concentration (MDA1), 98th percentile of hourly ozone concentrations (Perc98) and
263 4th highest MDA8 (4MDA8); (3) metrics that characterize ozone exposure: cumulative
264 hourly ozone concentrations of >40 ppb (AOT40) and sum of positive differences
265 between MDA8 and a cutoff concentration of 35 ppb (SOMO35); (4) The metrics that
266 characterize the days when the ozone exceeds the standard: total number of days with
267 MDA8 values of >70 ppb (NDGT70) and number of days with the ozone concentration
268 exceeding the Chinese grade II national air quality standard (Exceedance). Figure 2
269 presents variations in these four categories of ozone metrics at PKUERS site during the
270 study periods. The results show that overall all metrics increased during the 12 year
271 period. However, the percent increase, the p value and the correlation coefficient vary
272 between metrics. The median, DTAvg, and MDA8 indicators, which characterize the
273 general concentration levels of ozone, increased at rates of 2.8% - 5.7% yr^{-1} . The
274 metrics that characterize the extreme concentration levels of ozone increased more
275 slowly (1.2% - 2.7% yr^{-1}). Among them, Perc98 had the smallest rate of increase, only
276 1.2% yr^{-1} , and the correlation is not significant ($p = 0.29$, $r^2 = 0.11$). This indicates that

277 increases in the extreme ozone pollution was less significant. In contrast, the increase
278 rates of the ozone exposure metrics AOT40 and SOMO35 are faster, $8.4\% \text{ yr}^{-1}$ and 8.3%
279 yr^{-1} , respectively, than the metrics that characterize ozone concentrations. The NDGT70
280 and Exceedance metrics, related to the number of days of ozone exceeding the standard,
281 showed the fastest increases, $10\% \text{ yr}^{-1}$ and $9.8\% \text{ yr}^{-1}$, respectively.

282 As shown in Figure 3, from 2005 to 2016 MDA8 O₃ concentrations increased at a
283 rate of $2.3 \pm 1.2 \text{ ppbv}$ ($3.3 \pm 1.8 \%$) yr^{-1} ($r^2 = 0.66$) at the PKUERS site, which
284 corresponds to a total MDA8 ozone concentration increase of 25.3 ppbv. Meanwhile,
285 O_x (O₃+NO₂) concentrations increased at a slower rate of $1.4 \pm 0.6 \text{ ppbv}$ ($1.9 \pm 0.8 \%$)
286 yr^{-1} , due to the decrease in NO_x concentrations (Figure 5).

287 Temperature and wind speed, which can directly influence ozone production and
288 concentrations, showed no significant trend during 2005-2016 (Figure 4). The average
289 temperatures in summer were between 26 and 31°C. The temperature in 2005 was the
290 lowest and in 2007 it was the highest. The average wind speeds were less than 2.5 m s^{-1}
291 in all years. The average relative humidity may have decreased slightly ($\sim 1.5\% \text{ yr}^{-1}$).
292 In summary, we believe that meteorological factors did not play more than a minor role
293 in the overall Beijing O₃ trend. Therefore, our discussion focuses on photochemical
294 processes.

295 The ozone concentration observed at a receptor site depends on two
296 contributions: regional background ozone and local photochemical production. We
297 have no direct measurements of the long-term trend of regional background ozone in
298 Beijing, but others have reported measurements of ozone at regional background sites
299 in China. At a baseline Global Atmospheric Watch (GAW) station in the northeastern
300 Tibetan Plateau region (Mt Waliguan, 36.28° N, 100.9° E) the average annual daytime
301 ozone concentration increased at a rate of 0.24 ppb yr^{-1} , over the 1994 to 2013 period,
302 but there was no significant trend in summer (Xu et al., 2018). The measurement at a
303 rural station (Dingling site) in Beijing (116.22° E, 40.29° N, 34 km northwest of the
304 observation site in this study) showed a decrease of ozone at a rate of $-0.47 \text{ ppb yr}^{-1}$
305 over the 2004 to 2015 period (Zheng et al., 2016). The MDA8 ozone concentration at

306 the Shangdianzi site, a background station in Beijing, showed an increasing trend of
307 1.1 ppb yr⁻¹ during 2004-2014 (Ma et al., 2016a). Additionally, there were very small
308 trends of O₃ concentrations at the background site (Dongtan) in Shanghai, located to
309 the south of the North China Plain (Gao et al., 2017). However, these background
310 sites in Beijing and Shanghai may be strongly affected by local emissions. MDA8
311 ozone concentrations at the Changdao site, a background site in the east of the North
312 China Plain that is much less influenced by local emissions, increased slowly (+1.2
313 ppbv yr⁻¹, r²=0.11), but that rate is not statistically significant (p = 0.25) during 2013-
314 2019 (Figure S1). Based on these reports of smaller and variable trends, we assume
315 that the trend in regional background ozone in the North China Plain made only a
316 minor contribution to the relatively larger ozone trend observed at the PKUERS site
317 (+2.3 ± 1.2 ppbv yr⁻¹, r²=0.66, p = 0.001). We thus surmise that the increase in O₃ at
318 the PKUERS site was mainly due to “local” photochemistry driven by emissions of
319 ozone precursors from the central urban and surrounding suburban areas of Beijing.

320 **3.2 Trend of gaseous precursors**

321 This increase in ozone concentrations is opposite to the decreasing trend of its
322 precursors, including VOCs, CO and NO_x (Figure 5). The overall change of the total
323 OH loss rate due to VOCs (VOC reactivity) was -0.36 s⁻¹ (-6.0%) yr⁻¹. For
324 anthropogenic VOCs, the highest reactivity was generally contributed by alkene
325 species, with an average value over the eleven years of 2.00 ± 0.43 s⁻¹, followed by
326 aromatics and alkanes, with average reactivities of 1.51 ± 0.74 s⁻¹ and 0.92 ± 0.60 s⁻¹,
327 respectively. Thus, the alkenes and aromatics are more important for O₃ production
328 than are alkanes. The trends for alkenes, aromatics, and alkanes were a decrease of
329 0.14 s⁻¹ (7.1%), 0.12 s⁻¹ (7.9%), and 0.065s⁻¹ (7.0%) yr⁻¹, respectively, indicating that
330 alkenes and aromatics also played the dominant role in the reduction of anthropogenic
331 VOC reactivity. The rate of decrease in VOCs at PKUERS site is similar to that
332 reported for Los Angeles by Warneke et al. and Pollack et al. (7.3-7.5% yr⁻¹ over 50
333 years) (Warneke et al., 2012;Pollack et al., 2013). The decrease in anthropogenic

334 VOCs in Los Angeles was predominantly attributed to decreasing emissions from
335 motor vehicles due to increasingly strict emissions standards. Similarly, a previous
336 study at the PKUERS site indicated that the decreasing anthropogenic VOC was
337 mainly attributed to the reduction of gasoline evaporation and vehicular exhaust under
338 the implementation of stricter emissions standards for new vehicles and specific
339 control measures for in-use vehicles (Wang et al., 2015a). For naturally emitted
340 VOCs, mainly isoprene, the OH reactivity had little trend with large fluctuations, as
341 the emissions of plants vary greatly with temperature and light intensity. Therefore,
342 the decrease in total VOCs reactivity was dominated by the decrease in anthropogenic
343 VOCs. Similarly, CO, which is mainly contributed by anthropogenic emissions,
344 decreased rapidly ($9.3\% \text{ yr}^{-1}$) during 2006–2016.

345 NO_x data in 2005 were not available. Therefore, the trend of NO_x during 2006-
346 2016 was analyzed. Daytime concentrations of NO_x at the PKUER site also decreased
347 significantly from 2006 to 2016 (Figure 5), with a slope (excluding 2008, which had a
348 much lower NO_x concentration due to enhanced emission controls implemented during
349 the Olympic Games) of $-1.48 \text{ ppbv yr}^{-1}$ ($-5.5\% \text{ yr}^{-1}$, $r^2 = 0.81$). The decrease in NO_x
350 was mainly due to the reduction in vehicle exhaust and coal combustion (Zhao et al.,
351 2013). The decrease in NO_x was significantly faster than that found in Los Angeles by
352 Pollack et al. ($2.6\% \text{ yr}^{-1}$ over 50 years) (Pollack et al., 2013). In contrast to Beijing, Los
353 Angeles O₃ concentrations have continuously decreased from 1980 to 2010 (Parrish et
354 al., 2016). The ratio of the rates of decrease of VOCs and NO_x in Los Angeles (2.9) is
355 significantly greater than unity and larger than that at the PKUER site (1.1), which
356 possibly can be a contributing cause of the opposite trends of ozone in the two regions.
357 It worth noting that the precursor concentrations in 2008, the Olympic Games year,
358 were particularly low, but that ozone was nevertheless on the regression line. The
359 monthly average ratio of VOC reactivity to NO_x concentration in 2008 is $0.28 \text{ s}^{-1} \text{ ppbv}^{-1}$,
360 higher than the average ratio of VOC reactivity to NO_x concentration during 2006-
361 2016 ($0.24 \text{ s}^{-1} \text{ ppbv}^{-1}$). The adverse reduction ratio of VOC to NO_x is the main cause of
362 inefficient reduction in O₃ level in 2008, which is consistent with the study of Chou et

363 al. (2011).

364 Since 2013, under the implementation of the Action Plan on Air Pollution
365 Prevention and Control (http://www.gov.cn/zwggk/2013-09/12/content_2486773.htm),
366 more stringent emission control measures were implemented to restrict industrial and
367 vehicle emission. As a result, there are indications that both VOCs and NO_x decreased
368 faster over the 2013 to 2016 period: $0.81 \text{ s}^{-1} \text{ yr}^{-1}$ ($16\% \text{ yr}^{-1}$, $r^2 = 0.71$) and $1.94 \text{ ppbv yr}^{-1}$
369 ($9.3\% \text{ yr}^{-1}$, $r^2 = 0.78$) for VOC reactivity and NO_x, respectively. This could be the
370 cause of the decline in O₃ concentrations from 2014 to 2016.

371 **3.3 Trend of particulate matter**

372 From 2009 to 2016, PM_{2.5} concentrations declined rapidly, achieving the air
373 quality standard of China ($35 \mu\text{g}/\text{m}^3$) in 2016 (Figure 6). Since 2000, Beijing had
374 implemented 16 phases' air pollution control measures, mainly including the
375 controlling of industry, motor vehicle, coal combustion and fugitive dust pollution,
376 which was effective for the reduction in PM_{2.5} (Lang et al., 2017). Especially the
377 strengthening of the reduction in coal combustion, which was gradually replaced by
378 natural gas since 2004, favored improved visibility in Beijing (Zhao et al., 2011).

379 As shown in Figure 6, from 2006 to 2016 AOD decreased at a rate of $9.3\% \text{ yr}^{-1}$.
380 The correlation between AOD and PM_{2.5} can be determined from the observations of
381 PM_{2.5} and AOD in August during 2009-2016 at the PKUERS site (Figure 7). AOD
382 and PM_{2.5} are linearly correlated with a correlation coefficient of +0.74. This result
383 indicates that the decrease in PM_{2.5} was the primary cause of the reduction in AOD. In
384 addition to PM_{2.5}, relative humidity also has an important effect on AOD. The
385 decrease in relative humidity during 2006-2016 (Figure 4) would reduce the
386 hygroscopic growth of aerosol, leading to a weakened extinction effect of particulate
387 matter on solar radiation (Qu et al., 2015). It is worth noting that although PM_{2.5} in
388 2011 was lower than that in 2010, AOD in 2011 was higher than that in 2010 (Figure
389 6). For one reason, the relative humidity in 2011 was higher. Additionally, the aerosol
390 type, atmospheric boundary layer height and the vertical structure of aerosol

391 distribution also affects the dependence of AOD on PM_{2.5} (Zheng et al., 2017),
392 probably contributing to the scatter about the AOD versus PM_{2.5} relationship shown in
393 Figure 7.

394 Monthly mean AE (380/550 nm) in August showed no overall trend during 2006-
395 2016 (Figure 8). The monthly AE means were between 0.87 and 1.2, suggesting that
396 the size-distribution of aerosol was generally stable during this period. Monthly mean
397 SSA (440 nm) in August showed an upward trend of +0.004 yr⁻¹ (+0.45% yr⁻¹, p =
398 0.001) during 2006-2016 (Figure 8), indicating the proportion of the light-absorbing
399 component of aerosols (e.g. black carbon) has decreased, due to the stringent and
400 effective controls on the burning of biomass/biofuel and coal (Ni et al., 2014; Cheng et
401 al., 2013). This result is consistent with the studies of Lang et al. and Wang et al.,
402 which indicated that black carbon in China's mega cities has decreased rapidly over
403 the past decade (Wang et al., 2016b; Lang et al., 2017).

404 **3.4 Trend of photolysis frequencies**

405 The influence of solar radiation on O₃ photochemistry can be described by
406 actinic flux (or photolysis frequencies). We chose j(NO₂) as a representative
407 photolysis frequency to analyze the trend of actinic flux. Wang et al (2019) studied the
408 quantitative relationship between j(NO₂) and AOD at the PKUERS site, and found
409 that j(NO₂) and AOD showed a clear nonlinear negative correlation at a given SZA,
410 with slopes ranging from -1.3 to $-3.2 \times 10^{-3} \text{ s}^{-1}$ at AOD < 0.7, indicating a significant
411 extinction effect of AOD on actinic flux near the ground.

412 The j(NO₂) calculated by the TUV model under clear-sky conditions shows an
413 upward trend of 3.6% yr⁻¹ from 2005 to 2016 and agrees well with the 5 years of
414 observed values from 2011 to 2016 (Figure 6). According to sensitivity analysis of
415 TUV, the decrease in AOD plays a dominant role in the j(NO₂) increase, contributing
416 about 80% of the total. Additionally, the increase in SSA also contributes significantly
417 to j(NO₂) increase, contributing about 17%.

418 In addition to aerosol optical properties, the photolysis frequency in the planetary

419 boundary layer is affected by other factors, including cloud extinction, ground
420 reflection, absorption by gases such as O₃, and Rayleigh scattering by gases. The
421 ground reflection is relatively stable for different years in the same city with stable
422 ground covering. The change in Rayleigh scattering of gases and absorption of NO₂,
423 SO₂ and HCHO plays a negligible role in the variation in photolysis frequencies
424 according to sensitivity analysis of TUV model. This is consistent with the results of
425 Barnard et al. (Barnard et al., 2004). As shown in Figure 9, the total ozone column
426 fluctuated between 285-307 DU without a significant overall trend. The magnitude of
427 total ozone column variation (22 DU) can change j(O¹D) by about 10%, but plays a
428 negligible role in changing other photolysis frequencies according to sensitivity
429 analysis using the TUV model. The cloud optical thickness (COT) for most years was
430 relatively stable, ranging from 6 to 8, but in 2005, 2012 and 2015 COT was
431 significantly larger (Figure 9). As there was no significant trend of COT, we surmised
432 that the light-extinction effect of clouds did not play a key role in determining the
433 trend of photolysis frequencies.

434 **3.5 Combined effect of changes in ozone precursors and aerosols on ozone** 435 **production**

436 We investigated the overall effect of the changes in VOCs, NO_x, photolysis
437 frequency, and aerosol uptake of HO₂ on ozone production rate using the chemical
438 box model. We focus on the period during 2006-2016 due to the lack of NO_x data in
439 2005. By testing the response of P(O₃) as calculated from Equation E1 to the changes
440 of VOCs and NO_x concentrations (Figure 10), we concluded that photochemical
441 environment of the PKUERS site was, on average, in the VOC-limited regime. This
442 result is consistent with previous studies (Zhang et al., 2014;Chou et al., 2011). Under
443 this condition, the long-term decrease in VOCs in Beijing has contributed to a
444 decrease in P(O₃), while the decrease in NO_x has tended to increase P(O₃). As shown
445 in Figure 11, when the increase in photolysis frequencies and aerosol uptake of HO₂
446 were not included in the calculation, the simulated daytime average P(O₃) decreased

447 slightly at a rate of 1.1% yr⁻¹. This indicates that the ratio of the rates of decrease of
448 VOCs and NO_x (about 1.1) is nearly inefficient in reducing ozone production in
449 Beijing. However, when the increase in photolysis frequencies was included in the
450 model calculation, the calculated daytime average P(O₃) showed an increasing trend
451 of 2.2% yr⁻¹. This result indicates that the increase in photolysis frequencies more
452 than compensated for the downward trend of O₃ production driven by decreased
453 VOCs and NO_x, leading to increasing O₃ production through the decade. The
454 photochemical box model calculations indicate that the increase in photolysis
455 frequencies has two major impacts on P(O₃) - an increase in primary production of
456 OH through accelerated photolysis of O₃, HONO, HCHO and other carbonyl
457 compounds, and an accelerated radical recycling of OH as VOCs are oxidized. As
458 particulate matter has decreased and photolysis frequencies correspondingly have
459 increased, a more rapidly decreasing rate of the VOC to NO_x ratio is required to
460 achieve a significant reduction in O₃ in the future.

461 The simulated P(O₃) in the afternoon hour (12:00-15:00) when ozone production
462 is active and HO_x levels are high increased at a rate of 1.3% yr⁻¹, which is lower than
463 the increasing rate of daytime average P(O₃) (2.2% yr⁻¹) (Figure S2). Hollaway et al.
464 (2019) show that the impacts of aerosols on the summertime photolysis of NO₂ and
465 ozone at surface in Beijing are important before 11:00 am and after 3:00 pm but very
466 limited in afternoon hours due to smaller SZA and lower light absorption of aerosol
467 (i.e. higher SSA) in the afternoon. However, the diurnal variation of simulated P(O₃)
468 in this study indicates that the influence of aerosols on P(O₃) is still significant in the
469 afternoon, leading to average P(O₃) decreased by ~18% (Figure S3), which is slightly
470 lower than the mean daytime decrease (26%). This is because the average AOD in the
471 afternoon (1.4) is significantly higher than that before 11:00 am (0.94) and after 3:00
472 pm (1.1) despite the smaller SZA and higher SSA.

473

474 When we include heterogeneous uptake of HO₂ in the model, the calculated
475 P(O₃) increases at a faster rate of 2.9% yr⁻¹ due to the overall reduced aerosol surface

476 concentration (S_a), which reduces heterogeneous uptake of HO_2 (Figure 11). This
477 result indicates that the effect of heterogeneous uptake of HO_2 contributed roughly
478 $0.7\% \text{ yr}^{-1}$ to the $\text{P}(\text{O}_3)$ increase. Hence, our result indicates that the increase in
479 photolysis rates due to PM decrease plays a more important role than the decrease in
480 heterogeneous uptake of HO_2 by aerosols in accelerating ozone production in Beijing.
481 Previous measurements indicate that the uptake coefficient varies widely from 0.003
482 to 0.5 with a strong dependence on the aerosol concentration of transition metal ions
483 such as $\text{Cu}(\text{II})$ (Zou et al., 2019;Taketani et al., 2008;Lakey et al., 2015;Matthews et
484 al., 2014;Lakey et al., 2016). This strong dependence on aerosol composition implies
485 that a single assumed value for $\gamma_{\text{HO}_2} = 0.2$ has large uncertainty. $\gamma_{\text{HO}_2} = 0.2$ used in our
486 simulation is likely an overestimate of the effect of heterogeneous uptake of HO_2 on
487 ozone production rate at PKUERS site.

488 A few heterogeneous chemical reactions of nitrogen oxides are thought to be
489 potential influential factors of ozone production. For example, the heterogeneous
490 uptake of NO_2 to produce HNO_3 and HONO , and the heterogeneous uptake of NO_3
491 and N_2O_5 to produce HNO_3 . Our simulation indicates that the reduced heterogeneous
492 uptake of NO_x caused $\text{P}(\text{O}_3)$ to increase by only $\sim 2.2\%$ during 2006-2016. Li et al.
493 (2019a) also reported that the effect of heterogeneous uptake of nitrogen oxides on
494 ozone is very small under VOC-limited and summertime conditions in North China
495 Plain. Our simulated result in summertime Beijing, where VOC-limited
496 photochemistry dominates, is consistent with the result of Li et al. (2019a).

497 In summertime, PM in the Beijing urban area is mainly formed by the secondary
498 conversion of gaseous precursors (Han et al., 2015;Guo et al., 2014), indicating that
499 VOCs and NO_x are not only the precursors of ozone, but also the main precursors of
500 PM in this urban area. In addition, observations in Beijing have shown that the
501 secondary components of PM, including secondary organic matter, ammonium sulfate
502 and ammonium nitrate, dominate the light extinction of PM (Han et al., 2014;Han et al.,
503 2017;Wang et al., 2015b). As a result, reductions of VOCs and NO_x are expected to
504 lead to a decrease in secondary PM formation, and thus to further enhancement in solar

505 radiation (or actinic flux). Therefore, in order to reduce ozone effectively, the
506 contribution of VOCs and NO_x to secondary PM formation and their effect on solar
507 radiation must be comprehensively considered. However, the summertime formation of
508 PM is quite complex; the conversion efficiency of gaseous precursors to aerosols and
509 the resulting influence on ozone production is a research area that requires further study.

510 **3.6 Additional considerations**

511 One limitation of this study is that the photochemical box model is constrained
512 by surface observations, and hence may not accurately represent some aspects of the
513 photochemistry through the full depth of the planetary boundary layer over Beijing.
514 Here we briefly consider several of these aspects: (1) The treatment of ozone and
515 VOC and NO_x precursor concentrations likely are accurately represented, because
516 rapid daytime vertical mixing ensures that there is only a small vertical gradient in the
517 concentrations of these relatively long-lived species. (2) In daytime, the HONO
518 lifetime is so short that it may be largely confined to near the surface, where it has
519 surface sources (heterogeneous reaction of H₂O and NO₂ and emissions on surfaces).
520 Therefore, the estimated HONO based on near-surface NO₂ concentrations may
521 overestimate average boundary layer HONO concentrations; however, in this study
522 the influence of HONO on the calculation is relatively small, so this is not a large
523 source of error. (3) The model is constrained by surface measurements of photolysis
524 frequencies, but these surface measurements do not accurately quantify the actinic
525 flux throughout the boundary layer. Figure 12 presents the vertical profiles of $j(\text{NO}_2)$
526 simulated by the TUV model for aerosol properties representative of Beijing. A thick
527 layer of aerosol effectively reduces radiation at the bottom of the layer, but not at the
528 top, where radiation may be enhanced due to upward scattering from the aerosol
529 below (Dickerson et al., 1997; Jacobson, 1998). Overall, vertical average $j(\text{NO}_2)$
530 increased by 32% from 2006 to 2016, which is comparable to the surface increase
531 (36%). These simulations indicate that the increased trend of $j(\text{NO}_2)$ derived from
532 surface observations do approximate the trend through the entire boundary layer.

533 However, there is a shift in the vertical profile of $j(\text{NO}_2)$ that is important. The
534 crossing point between $j(\text{NO}_2)$ profile of 2006 and zero AOD profile is above PBL,
535 while in 2016 the $j(\text{NO}_2)$ profile crosses the zero AOD profile within the PBL. This
536 means that as the AOD is reduced further, changes in the vertical average $j(\text{NO}_2)$ will
537 be limited, since increases in $j(\text{NO}_2)$ near the top of the PBL will compensate for
538 decreases near the surface. Additionally, this also denotes that the role of $\text{PM}_{2.5}$ may
539 be more important under condition like 2006, but will be limited under condition like
540 2016 when there is offsetting effect for PBL ozone by vertical mixing caused by
541 larger ozone vertical gradient (Gao et al., 2020).

542 Quantitative studies suggested that, the impact of aerosols via affecting
543 photolysis rates on net ozone production (Cai, 2013; Wang et al., 2019; Castro et al.,
544 2001) is more than on surface ozone concentrations (Jacobson, 1998; Li et al.,
545 2011a; Li et al., 2011b; Wang et al., 2016a). Moreover, several different transport
546 model studies (Xing et al., 2017; Li et al., 2018a; Li et al., 2019c) also show that the
547 impact of $\text{PM}_{2.5}$ on summer surface ozone concentrations is not important, which is
548 different from the relatively large change of net ozone production in this study. There
549 are several possible causes of this difference: (1) The net ozone production
550 characterizes the local ozone production level but can't completely represent ozone
551 concentrations that are also influenced by regional transport of ozone (Streets et al.,
552 2007; Wang et al., 2020; Moghani et al., 2018). (2) The light-extinction effect of
553 aerosols lead to ozone at the top of PBL being entrained by turbulence to the surface
554 to partly counteract the reduction in surface ozone photochemical production induced
555 by aerosols (Gao et al., 2020). (3) AOD decreased by 58% in Beijing in this study,
556 which is higher than that of regional AOD decrease in eastern China (20%) (Li et al.,
557 2019b). (4) The photolysis rates in this study are determined using the observed AOD
558 SSA, and confirmed by ground-level measurements of photolysis frequencies, while
559 photolysis rates are determined using online algorithm in other transport model
560 studies. The different calculation procedures also contribute to the different results
561 between our study and other transport model studies.

562 **4 Conclusion**

563 During the past decade, China has devoted very substantial resources to
564 improving the environment. These efforts have improved atmospheric particulate
565 matter loading, but ambient ozone levels have continued to increase. Based on the
566 long-term measurements at a representative site in Beijing, we explored the factors
567 driving the increase in ozone production. Consistent with the implementation of
568 stringent emission control measures, concentrations of PM_{2.5} and ozone precursors
569 (VOCs and NO_x) decreased rapidly, but in contrast surface O₃ and O_x concentrations
570 increased. This investigation finds that the primary cause of the O₃ increase is that
571 decreasing PM concentrations led to an increase in actinic flux, which in turn
572 increased the photochemical production of ozone. This result indicates that the
573 influence of aerosol on ozone production is important for determining the full
574 manifold of atmospheric effects that result from reducing the emissions of the O₃ and
575 PM precursors.

576 **ACKNOWLEDGEMENTS**

577 This work was supported by the Major Program of the National Natural Science
578 Foundation of China [Grant number 91644222, Grant number 91644108]. We thank
579 Hongbin Chen and Philippe Goloub for data management of AOD and other aerosol
580 optical properties on AERONET.

581

582 **Data availability**

583 The data can be accessed upon contact with the corresponding authors.

584

585

586

587

588

589 **Author contribution**

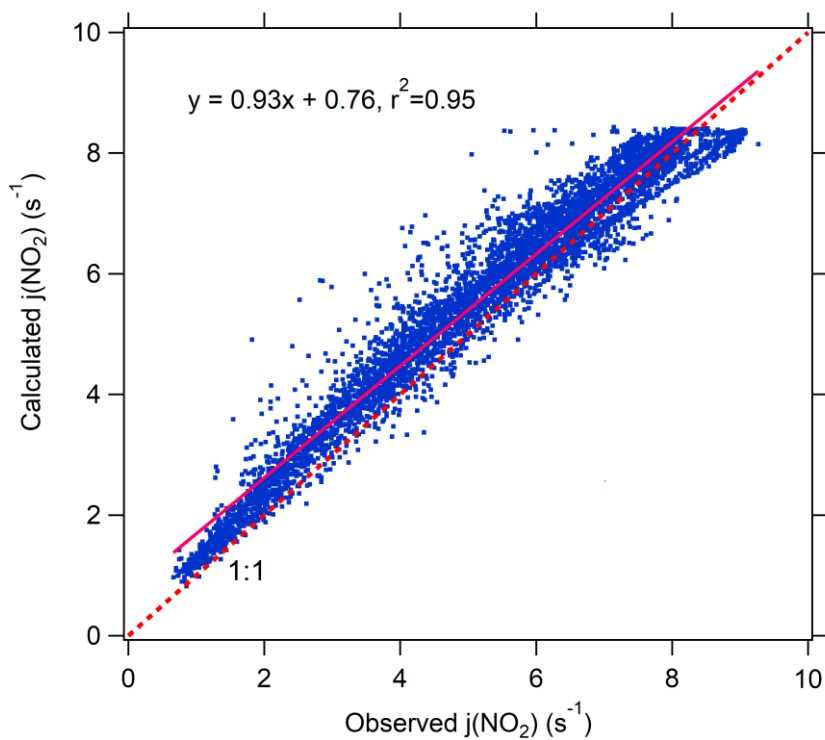
590 Wenjie Wang acquired, analyzed, and interpreted data, drafted the article, and
591 revised it critically. Xin Li substantially contributed to conception and design and
592 revised the article critically. David D. Parrish, Min Shao and Ziwei Mo revised the
593 article critically, Ying Liu, Sihua Lu, Min Hu, Xin Fang, Yusheng Wu, Limin Zeng
594 and Yuanhang Zhang collected data.

595

596 **Competing interests**

597 The authors declare that they have no conflict of interest.

598



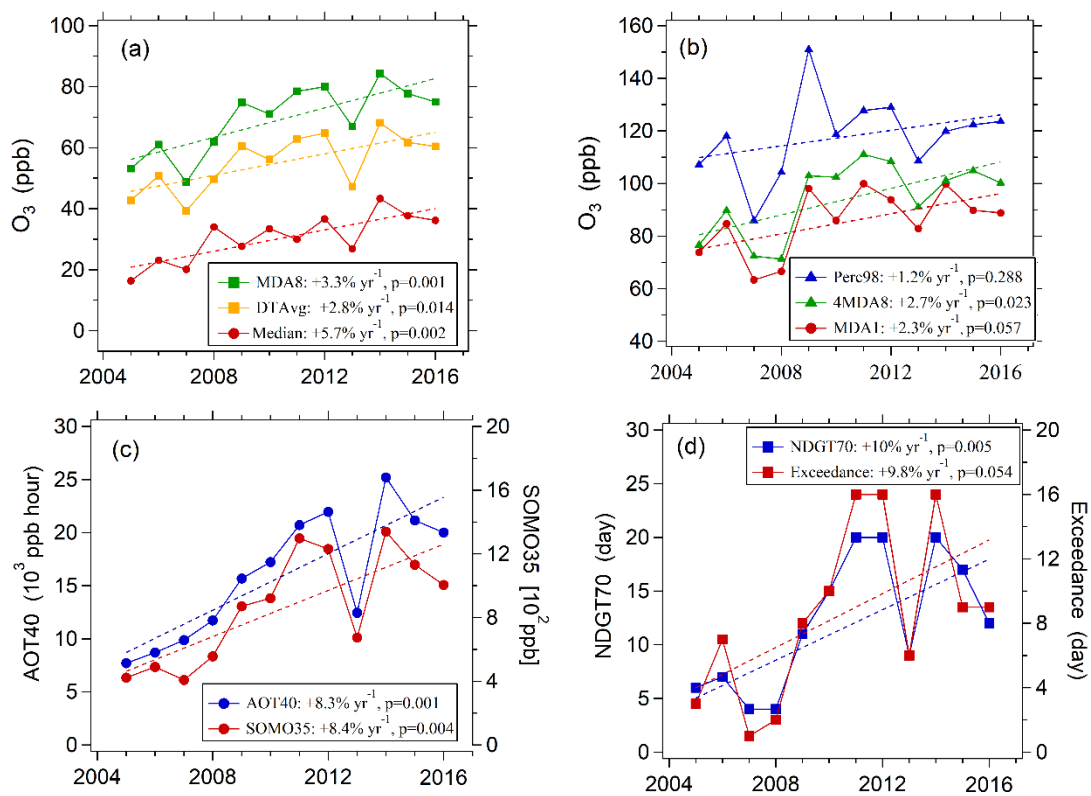
599

600 Figure 1. Correlation between Observed and calculated $j(\text{NO}_2)$ by TUV model in

601 Beijing in summer time during 2012 - 2015.

602

603



604

605

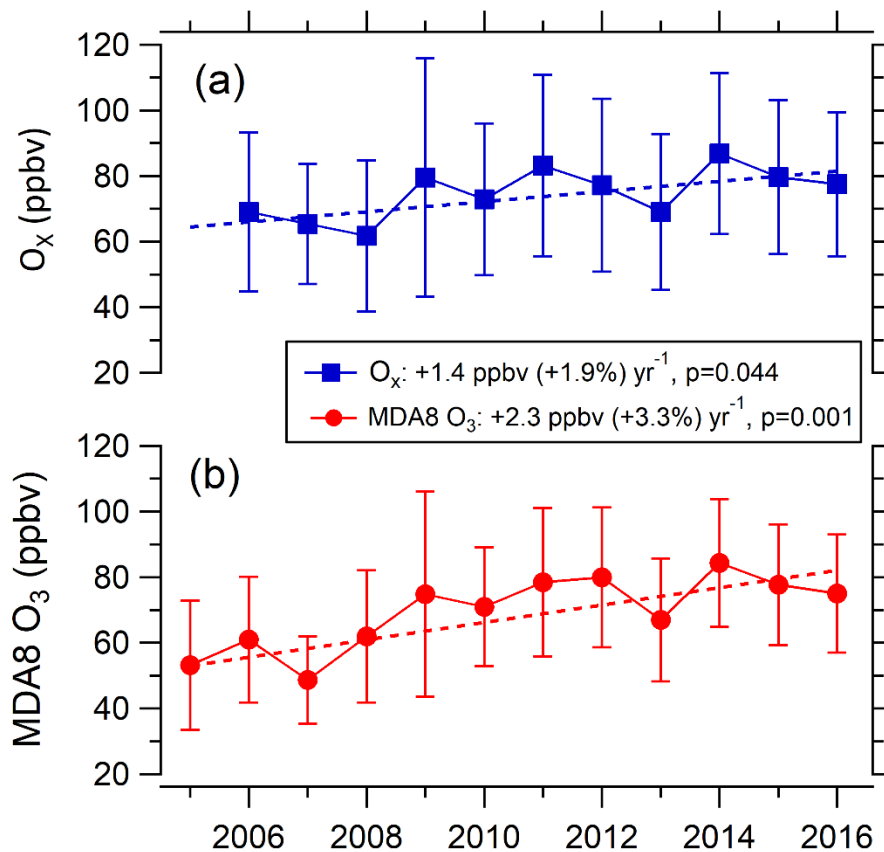
Figure 2. Variations in multiple O_3 metrics at the PKUERS site in Beijing in August between 2005 and 2016.

606

607

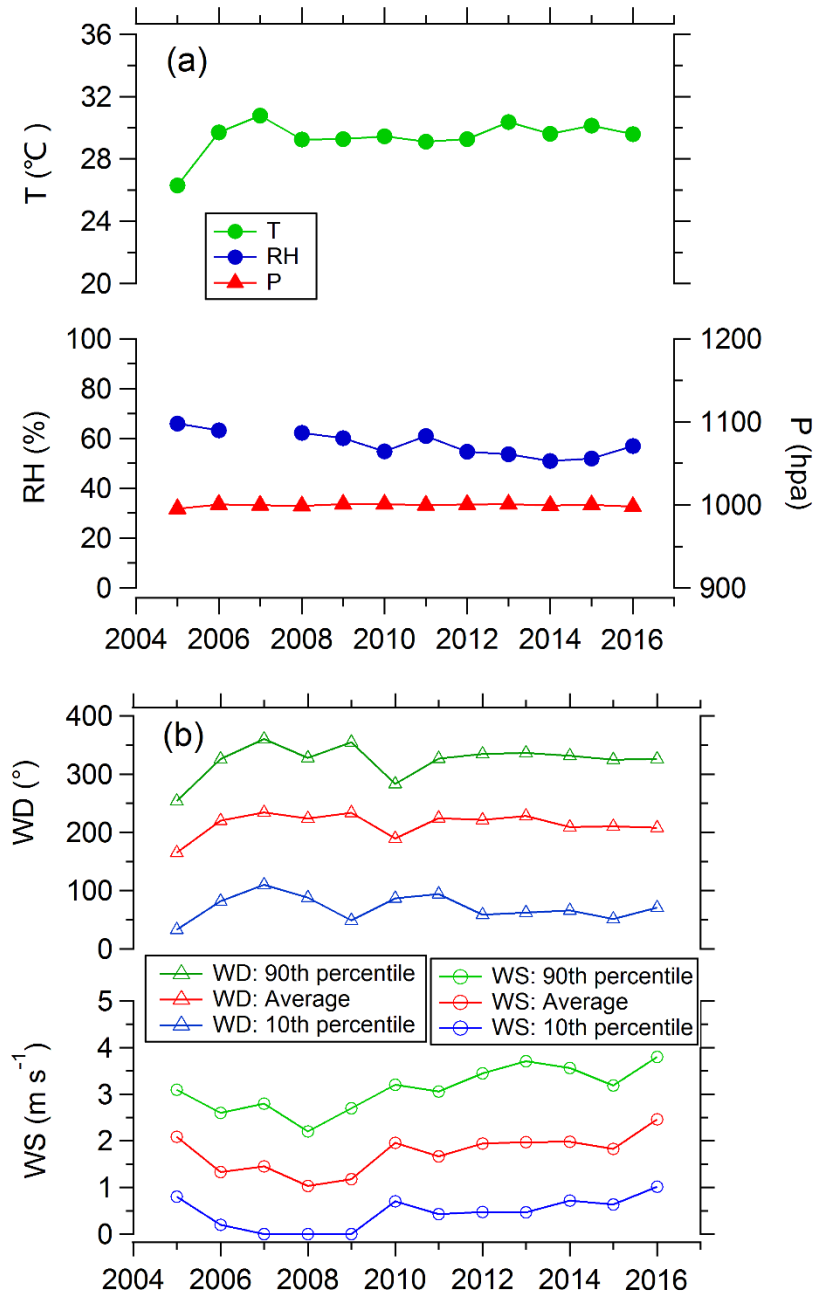
608

609
610



611
612
613
614

Figure 3. Variations in average MDA8 O₃ and daytime (7:00-19:00) average Ox in Beijing, August between 2005 and 2016.



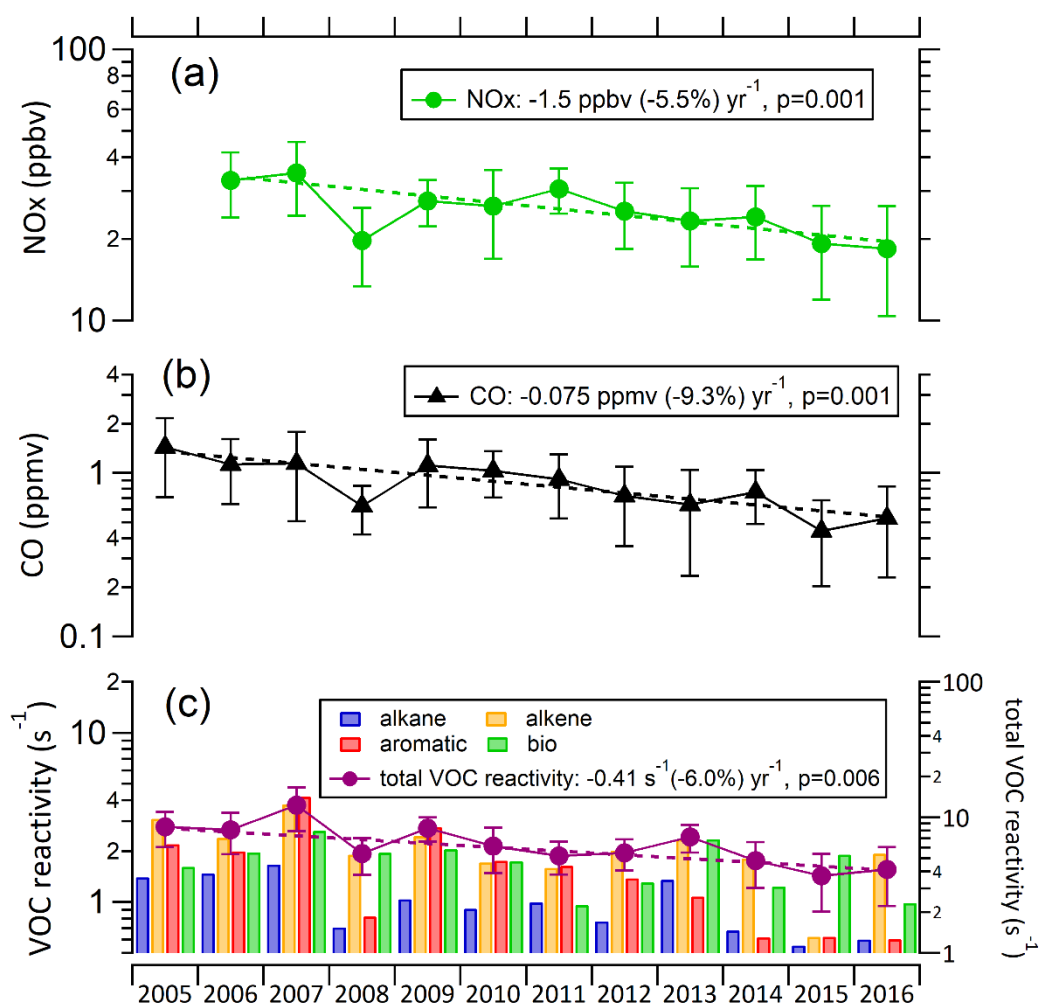
615

616 Figure 4. Variations in daytime (7:00-19:00) averages of meteorological conditions
 617 including temperature (T), relative humidity (RH), wind direction (WD) and wind
 618 speed (WS) in Beijing, August during 2005 - 2016.

619

620

621



622

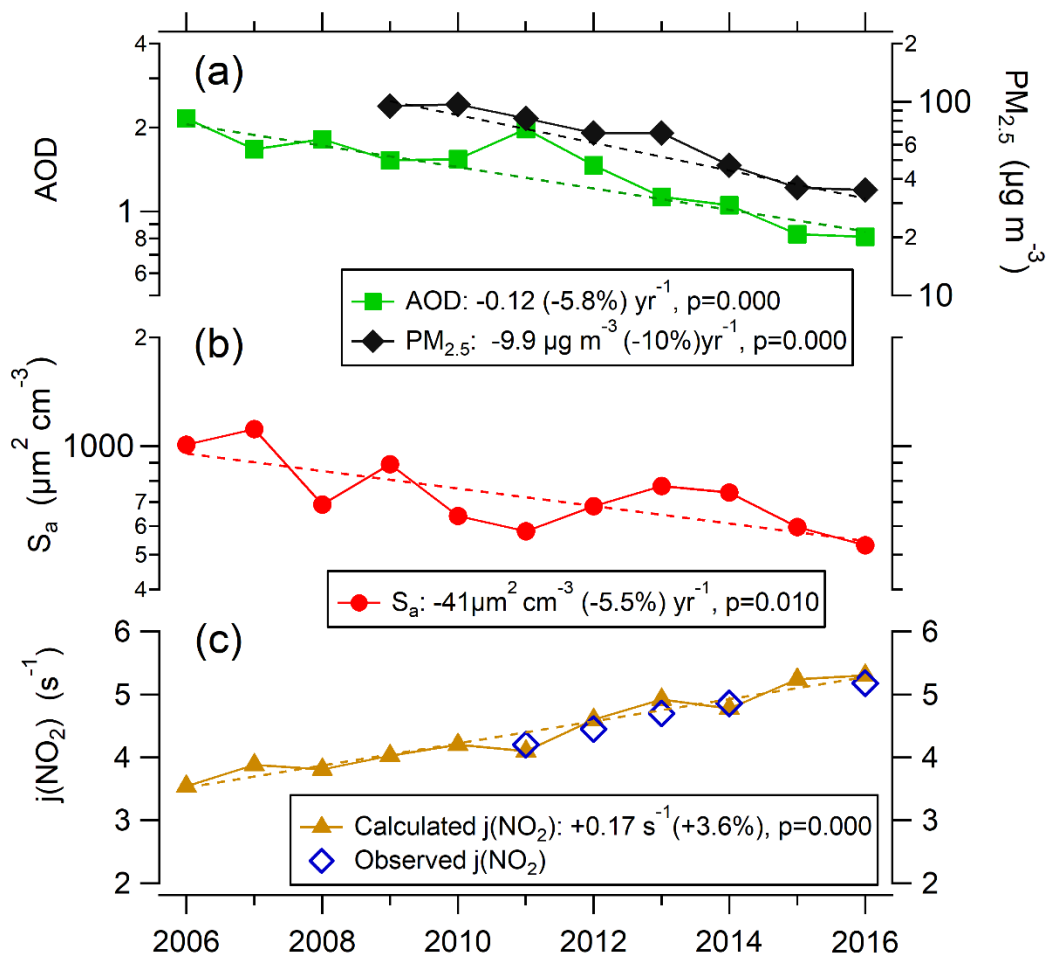
623 Figure 5. Variations in geometric mean of daytime NO_x, CO and VOCs reactivity in

624 Beijing, August between 2005 and 2016. VOCs reactivity is depicted by reactivity of

625 each species (left axis) and total VOC reactivity (right axis). On the y-axes, a log-

626 scale is used.

627



628

629 Figure 6. Variations in daytime (7:00-19:00) averages of AOD (380 nm), PM_{2.5}, S_a,

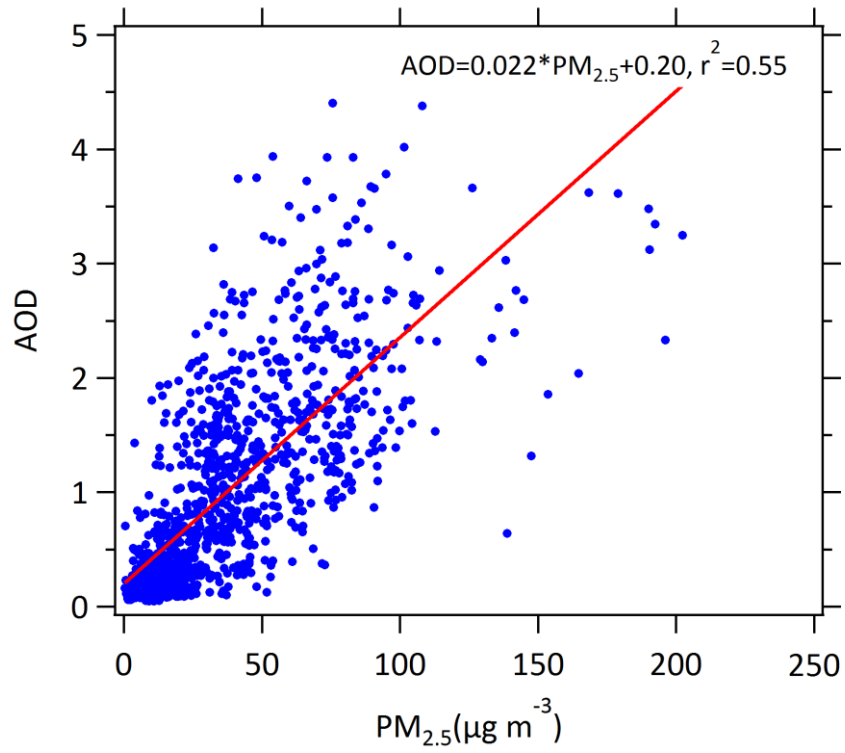
630 j(NO₂) Calculated j(NO₂) by TUV in Beijing, August between 2006 and 2016. AOD

631 and j(NO₂) are both corresponding to cloudless weather. On the y-axes, a log-scale is

632 used for PM_{2.5}, AOD and S_a and a linear scale is used for j(NO₂).

633

634

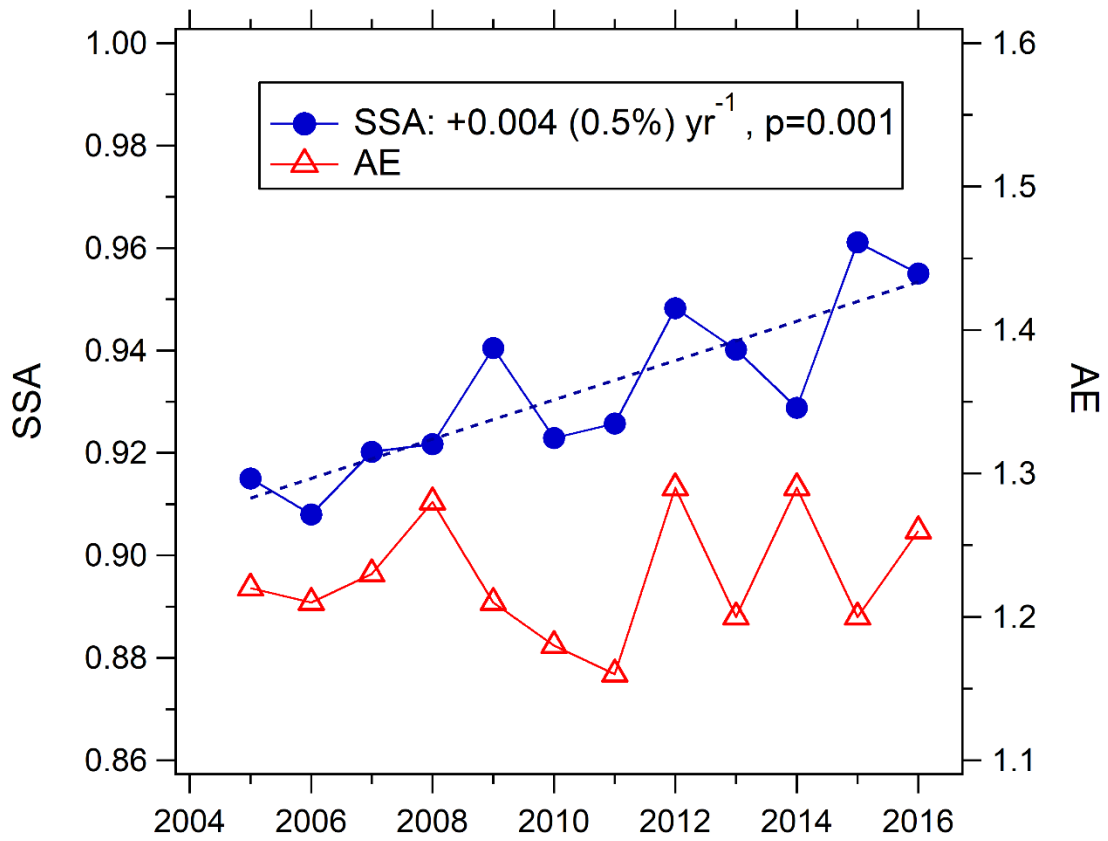


635

636 Figure 7. Correlation between AOD and PM_{2.5} in Beijing, summertime during 2009 -

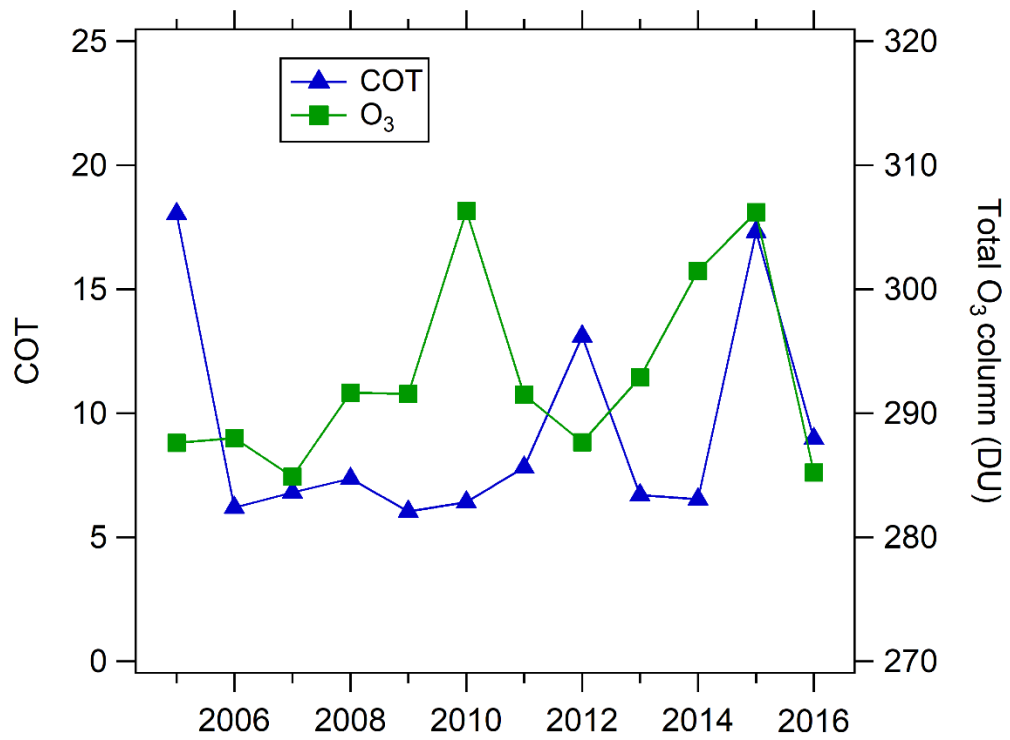
637 2016.

638



639
 640
 641
 642
 643
 644

Figure 8. Variation in monthly mean single scattering albedo (SSA) and Ångström exponent (AE) in Beijing for the month of August during 2005 - 2016.



645

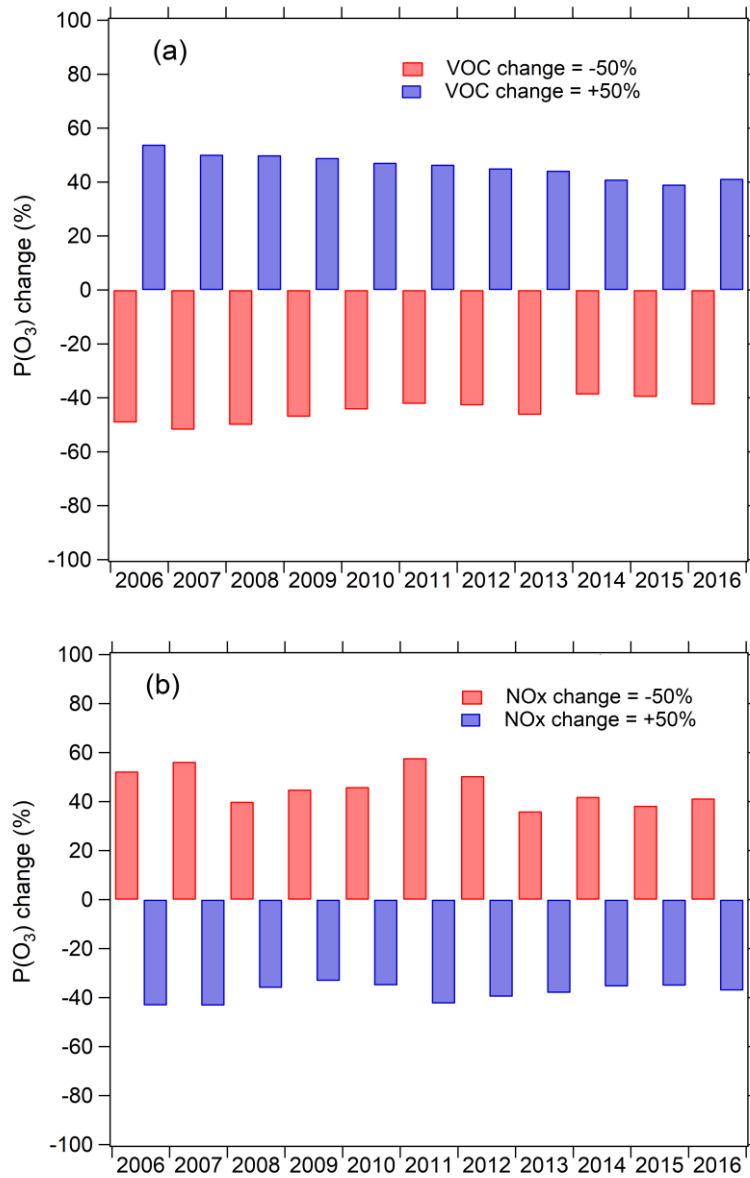
646 Figure 9. Variations in mean total ozone column and cloud optical thickness (COT) in

647 Beijing for the month of August during 2005 - 2016.

648

649

650

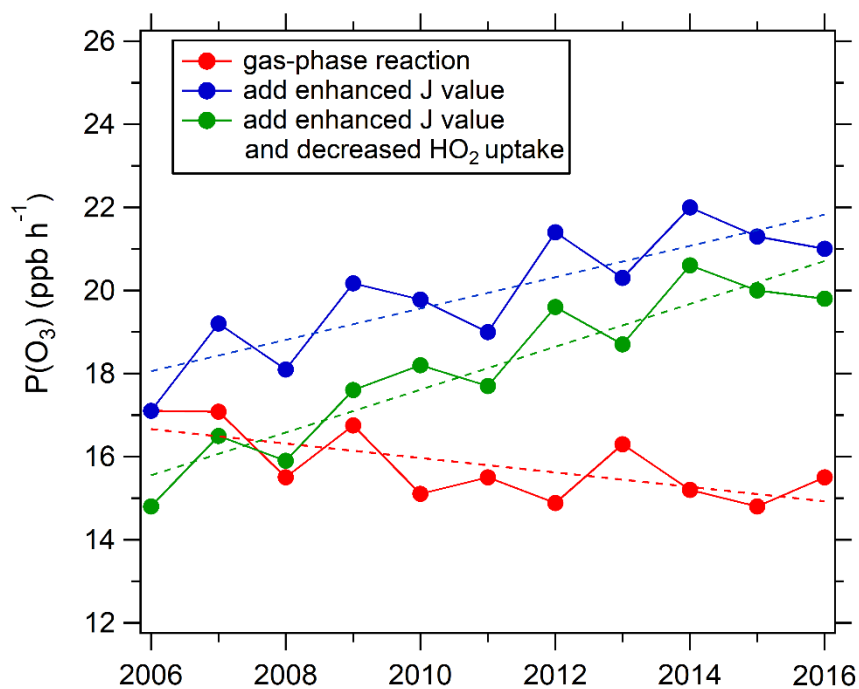


651

652 Figure 10. Sensitivity of monthly daytime mean $P(O_3)$ to VOCs and NO_x simulated
 653 by box model during 2006 - 2016. VOCs and NO_x is increased by 50% or decreased
 654 by 50% to test the fractional change of monthly daytime mean $P(O_3)$.

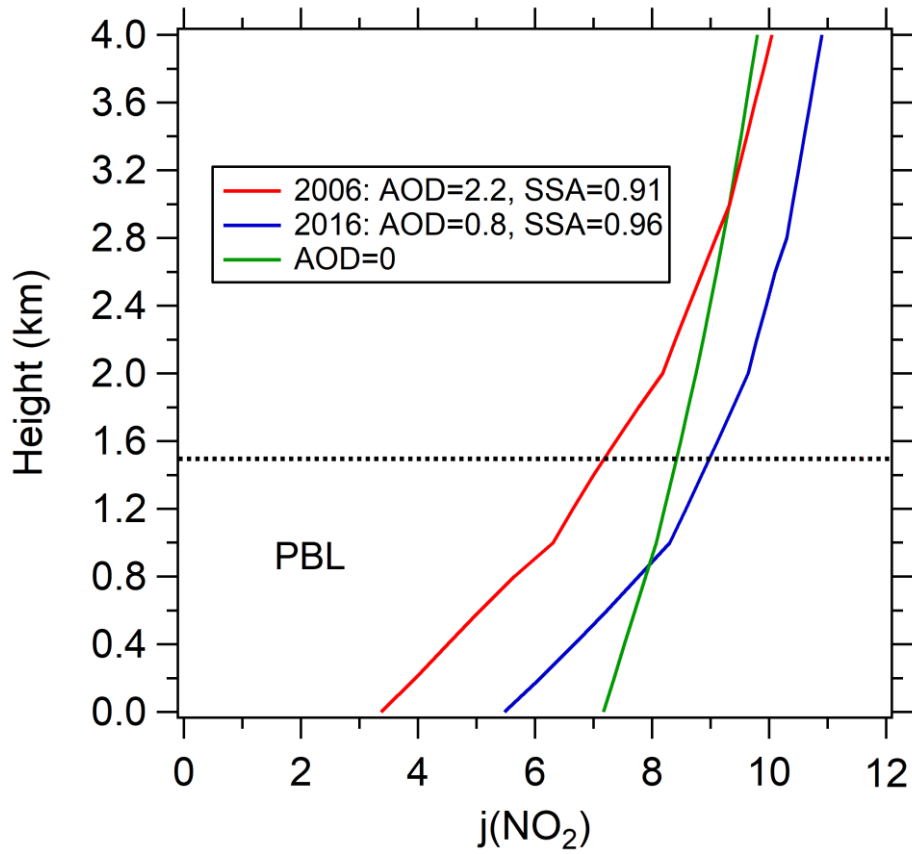
655

656



657

658 Figure 11. Trend of monthly daytime mean $P(O_3)$ simulated by the chemical box
659 model. Red dots: Only the gas-phase reactions are considered in the box model
660 constrained by observed photolysis frequencies from 2006 for all eleven years. Blue
661 dots: the box model as above, but constrained by the photolysis frequencies derived
662 for each year. Green dots: the box model constrained by the photolysis frequencies
663 derived for each year with the changing aerosol uptake of HO_2 also considered.
664



665

666 Figure 12. Vertical profiles of $j(\text{NO}_2)$ simulated by the TUV model in Beijing. Three
 667 scenarios are simulated: The model parameters are: (1) AOD=2.2, SSA=0.91 in August
 668 2006; (2) AOD=0.8, SSA=0.96 in August 2016; (3) AOD=0. The daytime average
 669 SZA=53° is used for all simulations. Dotted line represent the top of boundary layer.

670

671

672 Table 1. Instruments deployed in the measurement undertaken in August during 2005 -
 673 2016 and used for data analysis.

Parameters	Measurement technique	Time resolution	Detection limit	Accuracy
Photolysis frequencies	Spectroradiometer	10 s	/	± 10%
O ₃	UV photometry	60 s	0.5 ppbv	± 5%
NO	Chemiluminescence	60 s	60 pptv	± 20%
NO ₂	Chemiluminescence	60 s	300 pptv	± 20%
CO	IR photometry	60 s	4 ppb	± 5%
SO ₂	Pulsed UV fluorescence	60 s	0.1 ppbv	± 5%
HCHO	Hantzsch fluorimetry	60 s	25 pptv	± 5%
C2-C10VOCs	GC-FID/MS	1 h	20-300 pptv	± 15~20%
PM _{2.5}	TH-2000	60s	1µg m ⁻³	± 5%
S _a	SMPS	60s	/	±3%
AOD, SSA, AE	CIMEL Sun photometer	5min	0.01	±5%

674

675

676

Table 2. p value of temporal trends for different parameters.

Parameter	Period	r ²	p value	P value <0.01?	P value <0.05?
median	2005-2016	0.63	0.002	yes	yes
perc98	2005-2016	0.11	0.288	no	no
DTAvg	2005-2016	0.47	0.014	no	yes
MDA1	2005-2016	0.32	0.057	no	no
MDA8	2005-2016	0.66	0.001	yes	yes
4MDA8	2005-2016	0.42	0.023	no	yes
AOT40	2005-2016	0.67	0.001	yes	yes
NDGT70	2005-2016	0.56	0.005	yes	yes
SOMO35	2005-2016	0.57	0.004	yes	yes
exceedance	2005-2016	0.32	0.054	no	no
Ox	2005-2016	0.38	0.044	no	yes
CO	2005-2016	0.87	0.001	yes	yes
VOC reactivity	2005-2016	0.52	0.006	yes	yes
NO _x	2006-2016	0.81	0.001	yes	yes
Calculated j(NO ₂)	2006-2016	0.94	0.000	yes	yes
AOD (380 nm)	2006-2016	0.78	0.000	yes	yes
PM _{2.5}	2009-2016	0.93	0.000	yes	yes
Sa	2006-2016	0.51	0.010	yes	yes
SSA	2005-2016	0.70	0.001	yes	yes
AE	2005-2016	0.03	0.593	no	no
COT	2005-2016	0.003	0.875	no	no
Total O ₃ column	2005-2016	0.15	0.215	no	no

677

678

679

680

681

682

683

684

685

686

687

688

689 Table 3. Description of Ozone Metrics used in this study.

categories	metric	definition
general level	median (ppb)	50th percentile of hourly concentrations
	MDA8 (ppb)	daily maximum 8 h average; the mean MDA8 O ₃ in August of each year is used in this study.
	DTAvg (ppb)	daytime average ozone is the average of hourly ozone concentrations for the 12 h period from 07:00 to 19:00 local time
extreme level	MDA1 (ppb)	daily maximum 1 h average; the mean MDA1 O ₃ in August of each year is used in this study.
	Perc98 (ppb)	98th percentile of hourly concentrations
	4MDA8 (ppb)	4th highest MDA8
ozone exposure	AOT40 (ppb h)	cumulative hourly ozone concentrations of >40 ppb
	SOMO35 (ppb day)	sum of positive differences between MDA8 and a cutoff concentration of 35 ppb
Exceedance days	NDGT70 (day)	total number of days with MDA8 values of >70 ppb
	Exceedance (day)	number of days with the ozone concentration exceeding the Chinese grade II national air quality standard, defined as MDA8 > 160 µg m ⁻³

690

691

692 **References**

- 693 Atkinson, R.: Atmospheric chemistry of VOCs and NO_x, *Atmos. Environ.*, 34, 2063-
694 2101, 2000.
- 695 Barnard, J. C., Chapman, E. G., Fast, J. D., Schmelzer, J. R., Slusser, J. R., and Shetter,
696 R. E.: An evaluation of the FAST-J photolysis algorithm for predicting nitrogen
697 dioxide photolysis rates under clear and cloudy sky conditions, *Atmos. Environ.*,
698 38, 3393-3403, <https://doi.org/10.1016/j.atmosenv.2004.03.034>, 2004.
- 699 Bohn, B., Corlett, G. K., Gillmann, M., Sanghavi, S., Stange, G., Tensing, E.,
700 Vrekoussis, M., Bloss, W. J., Clapp, L. J., Kortner, M., Dorn, H. P., Monks, P. S.,
701 Platt, U., Plass-Dulmer, C., Mihalopoulos, N., Heard, D. E., Clemitshaw, K. C.,
702 Meixner, F. X., Prevot, A. S. H., and Schmitt, R.: Photolysis frequency
703 measurement techniques: results of a comparison within the ACCENT project,
704 *Atmospheric Chemistry and Physics*, 8, 5373-5391, 10.5194/acp-8-5373-2008,
705 2008.
- 706 Cai, Y. F., Wang, T. J., and Xie, M.: Impacts of atmospheric particles on surface ozone
707 in Nanjing (In Chinese), *Climatic Environment Research*, 18, 251-260,
708 10.5194/acp-8-6155-2008, 2013.
- 709 Castro, T., Madronich, S., Rivale, S., Muhlia, A., and Mar, B.: The influence of aerosols
710 on photochemical smog in Mexico City, *Atmos. Environ.*, 35, 1765-1772,
711 [https://doi.org/10.1016/S1352-2310\(00\)00449-0](https://doi.org/10.1016/S1352-2310(00)00449-0), 2001.
- 712 Cheng, Y., Engling, G., He, K. B., Duan, F. K., Ma, Y. L., Du, Z. Y., Liu, J. M., Zheng,
713 M., and Weber, R. J.: Biomass burning contribution to Beijing aerosol, *Atmos.*
714 *Chem. Phys.*, 13, 7765-7781, 10.5194/acp-13-7765-2013, 2013.
- 715 Chou, C. C. K., Tsai, C. Y., Chang, C. C., Lin, P. H., Liu, S. C., and Zhu, T.:
716 Photochemical production of ozone in Beijing during the 2008 Olympic Games,
717 *Atmos. Chem. Phys.*, 11, 9825-9837, 10.5194/acp-11-9825-2011, 2011.
- 718 de Miranda, R. M., Andrade, M. D., and Fattori, A. P.: Preliminary studies of the effect
719 of aerosols on nitrogen dioxide photolysis rates in the city of Sao Paulo, Brazil,
720 *Atmospheric Research*, 75, 135-148, 10.1016/j.atmosres.2004.12.004, 2005.
- 721 Dickerson, R. R., Kondragunta, S., Stenchikov, G., Civerolo, K. L., Doddridge, B. G.,
722 and Holben, B. N.: The Impact of Aerosols on Solar Ultraviolet Radiation and
723 Photochemical Smog, *Science*, 278, 827-830, 10.1126/science.278.5339.827,
724 1997.
- 725 Dubovik, O., and King, M. D.: A flexible inversion algorithm for retrieval of aerosol
726 optical properties from Sun and sky radiance measurements, *Journal of*
727 *Geophysical Research-Atmospheres*, 105, 20673-20696, 10.1029/2000jd900282,
728 2000.
- 729 Fiore, A. M., Dentener, F. J., Wild, O., Cuvelier, C., Schultz, M. G., Hess, P., Textor, C.,
730 Schulz, M., Doherty, R. M., Horowitz, L. W., MacKenzie, I. A., Sanderson, M. G.,
731 Shindell, D. T., Stevenson, D. S., Szopa, S., Van Dingenen, R., Zeng, G., Atherton,
732 C., Bergmann, D., Bey, I., Carmichael, G., Collins, W. J., Duncan, B. N., Faluvegi,
733 G., Folberth, G., Gauss, M., Gong, S., Hauglustaine, D., Holloway, T., Isaksen, I.

734 S. A., Jacob, D. J., Jonson, J. E., Kaminski, J. W., Keating, T. J., Lupu, A., Marmer,
735 E., Montanaro, V., Park, R. J., Pitari, G., Pringle, K. J., Pyle, J. A., Schroeder, S.,
736 Vivanco, M. G., Wind, P., Wojcik, G., Wu, S., and Zuber, A.: Multimodel estimates
737 of intercontinental source-receptor relationships for ozone pollution, *Journal of*
738 *Geophysical Research-Atmospheres*, 114, 21, 10.1029/2008jd010816, 2009.

739 Fotiadi, A., Hatzianastassiou, N., Drakakis, E., Matsoukas, C., Pavlakis, K. G.,
740 Hatzidimitriou, D., Gerasopoulos, E., Mihalopoulos, N., and Vardavas, I.: Aerosol
741 physical and optical properties in the Eastern Mediterranean Basin, Crete, from
742 Aerosol Robotic Network data, *Atmospheric Chemistry and Physics*, 6, 5399-5413,
743 10.5194/acp-6-5399-2006, 2006.

744 Gao, J., Li, Y., Zhu, B., Hu, B., Wang, L., and Bao, F.: What have we missed when
745 studying the impact of aerosols on surface ozone via changing photolysis rates?,
746 *Atmos. Chem. Phys. Discuss.*, 2020, 1-28, 10.5194/acp-2020-140, 2020.

747 Gao, W., Tie, X. X., Xu, J. M., Huang, R. J., Mao, X. Q., Zhou, G. Q., and Chang, L.
748 Y.: Long-term trend of O₃ in a mega City (Shanghai), China: Characteristics,
749 causes, and interactions with precursors, *Science of the Total Environment*, 603,
750 425-433, 10.1016/j.scitotenv.2017.06.099, 2017.

751 Gerasopoulos, E., Kazadzis, S., Vrekoussis, M., Kouvarakis, G., Liakakou, E.,
752 Kouremeti, N., Giannadaki, D., Kanakidou, M., Bohn, B., and Mihalopoulos, N.:
753 Factors affecting O₃ and NO₂ photolysis frequencies measured in the eastern
754 Mediterranean during the five-year period 2002-2006, *J. Geophys. Res.-Atmos.*,
755 117, 14, 10.1029/2012jd017622, 2012.

756 Goliff, W. S., Stockwell, W. R., and Lawson, C. V.: The regional atmospheric chemistry
757 mechanism, version 2, *Atmospheric Environment*, 68, 174-185,
758 10.1016/j.atmosenv.2012.11.038, 2013.

759 Guo, S., Hu, M., Zamora, M. L., Peng, J., Shang, D., Zheng, J., Du, Z., Wu, Z., Shao,
760 M., Zeng, L., Molina, M. J., and Zhang, R.: Elucidating severe urban haze
761 formation in China, *Proceedings of the National Academy of Sciences*, 111,
762 17373-17378, 10.1073/pnas.1419604111, 2014.

763 Han, T. T., Liu, X. G., Zhang, Y. H., Qu, Y., Gu, J. W., Ma, Q., Lu, K. D., Tian, H. Z.,
764 Chen, J., Zeng, L. M., Hu, M., and Zhu, T.: Characteristics of Aerosol Optical
765 Properties and Their Chemical Apportionments during CAREBeijing 2006,
766 *Aerosol Air Qual. Res.*, 14, 1431-1442, 10.4209/aaqr.2013.06.0203, 2014.

767 Han, T. T., Liu, X. G., Zhang, Y. H., Qu, Y., Zeng, L. M., Hu, M., and Zhu, T.: Role of
768 secondary aerosols in haze formation in summer in the Megacity Beijing, *Journal*
769 *of Environmental Sciences*, 31, 51-60, 10.1016/j.jes.2014.08.026, 2015.

770 Han, T. T., Xu, W. Q., Li, J., Freedman, A., Zhao, J., Wang, Q. Q., Chen, C., Zhang, Y.
771 J., Wang, Z. F., Fu, P. Q., Liu, X. G., and Sun, Y. L.: Aerosol optical properties
772 measurements by a CAPS single scattering albedo monitor: Comparisons between
773 summer and winter in Beijing, China, *Journal of Geophysical Research-*
774 *Atmospheres*, 122, 2513-2526, 10.1002/2016jd025762, 2017.

775 Hendrick, F., Muller, J. F., Clemer, K., Wang, P., De Maziere, M., Fayt, C., Gielen, C.,
776 Hermans, C., Ma, J. Z., Pinardi, G., Stavrou, T., Vlemmix, T., and Van
777 Roozendaal, M.: Four years of ground-based MAX-DOAS observations of HONO

778 and NO₂ in the Beijing area, *Atmospheric Chemistry and Physics*, 14, 765-781,
779 10.5194/acp-14-765-2014, 2014.

780 Hollaway, M., Wild, O., Yang, T., Sun, Y., Xu, W., Xie, C., Whalley, L., Slater, E., Heard,
781 D., and Liu, D.: Photochemical impacts of haze pollution in an urban environment,
782 *Atmospheric Chemistry and Physics*, 19, 9699-9714, 2019.

783 Hu, B., Zhao, X., Liu, H., Liu, Z., Song, T., Wang, Y., Tang, L., Xia, X., Tang, G., Ji,
784 D., Wen, T., Wang, L., Sun, Y., and Xin, J.: Quantification of the impact of aerosol
785 on broadband solar radiation in North China, *Scientific Reports*, 7, 44851,
786 10.1038/srep44851, 2017.

787 Jacob, D. J.: Heterogeneous chemistry and tropospheric ozone, *Atmos. Environ.*, 34,
788 2131-2159, 2000.

789 Jacobson, M. Z.: Studying the effects of aerosols on vertical photolysis rate coefficient
790 and temperature profiles over an urban airshed, *Journal of Geophysical Research:*
791 *Atmospheres*, 103, 10593-10604, 10.1029/98jd00287, 1998.

792 Jinfeng, Keding, Liuju, Zhong, Yubo, Duohong, Chen, Huang, Yuanhang, and Zhang:
793 Fast increasing of surface ozone concentrations in Pearl River Delta characterized
794 by a regional air quality monitoring network during 2006-2011, *Journal of*
795 *Environmental Sciences*, 26, 23-36, 2014.

796 Lakey, P. S. J., George, I. J., Whalley, L. K., Baeza-Romero, M. T., and Heard, D. E.:
797 Measurements of the HO₂ Uptake Coefficients onto Single Component Organic
798 Aerosols, *Environ. Sci. Technol.*, 49, 4878-4885, 10.1021/acs.est.5b00948, 2015.

799 Lakey, P. S. J., George, I. J., Baeza-Romero, M. T., Whalley, L. K., and Heard, D. E.:
800 Organics Substantially Reduce HO₂ Uptake onto Aerosols Containing Transition
801 Metal ions, *Journal of Physical Chemistry A*, 120, 1421-1430,
802 10.1021/acs.jpca.5b06316, 2016.

803 Lang, J. L., Zhang, Y. Y., Zhou, Y., Cheng, S. Y., Chen, D. S., Guo, X. U., Chen, S., Li,
804 X. X., Xing, X. F., and Wang, H. Y.: Trends of PM_{2.5} and Chemical Composition
805 in Beijing, 2000-2015, *Aerosol Air Qual. Res.*, 17, 412-425,
806 10.4209/aaqr.2016.07.0307, 2017.

807 Li, G., Bei, N., Tie, X., and Molina, L. T.: Aerosol effects on the photochemistry in
808 Mexico City during MCMA-2006/MILAGRO campaign, *Atmos. Chem. Phys.*, 11,
809 5169-5182, 10.5194/acp-11-5169-2011, 2011a.

810 Li, J., Wang, Z., Wang, X., Yamaji, K., Takigawa, M., Kanaya, Y., Pochanart, P., Liu,
811 Y., Irie, H., and Hu, B.: Impacts of aerosols on summertime tropospheric
812 photolysis frequencies and photochemistry over Central Eastern China, *Atmos.*
813 *Environ.*, 45, 1817-1829, 2011b.

814 Li, J., Chen, X., Wang, Z., Du, H., Yang, W., Sun, Y., Hu, B., Li, J., Wang, W., and
815 Wang, T.: Radiative and heterogeneous chemical effects of aerosols on ozone and
816 inorganic aerosols over East Asia, *Science of the Total Environment*, 622, 1327-
817 1342, 2018a.

818 Li, J., Chen, X. S., Wang, Z. F., Du, H. Y., Yang, W. Y., Sun, Y. L., Hu, B., Li, J. J.,
819 Wang, W., Wang, T., Fu, P. Q., and Huang, H. L.: Radiative and heterogeneous
820 chemical effects of aerosols on ozone and inorganic aerosols over East Asia,
821 *Science of the Total Environment*, 622, 1327-1342,

822 10.1016/j.scitotenv.2017.12.041, 2018b.

823 Li, K., Jacob, D. J., Liao, H., Shen, L., Zhang, Q., and Bates, K. H.: Anthropogenic
824 drivers of 2013–2017 trends in summer surface ozone in China, *Proceedings of*
825 *the National Academy of Sciences*, 116, 422-427, 2019a.

826 Li, K., Jacob, D. J., Liao, H., Shen, L., Zhang, Q., and Bates, K. H.: Anthropogenic
827 drivers of 2013-2017 trends in summer surface ozone in China, *Proceedings of the*
828 *National Academy of Sciences of the United States of America*, 116, 422-427,
829 10.1073/pnas.1812168116, 2019b.

830 Li, K., Jacob, D. J., Liao, H., Zhu, J., Shah, V., Shen, L., Bates, K. H., Zhang, Q., and
831 Zhai, S.: A two-pollutant strategy for improving ozone and particulate air quality
832 in China, *Nature Geoscience*, 12, 906-910, 10.1038/s41561-019-0464-x, 2019c.

833 Liu, X., Zhang, Y., Jung, J., Gu, J., Li, Y., Guo, S., Chang, S.-Y., Yue, D., Lin, P., Kim,
834 Y. J., Hu, M., Zeng, L., and Zhu, T.: Research on the hygroscopic properties of
835 aerosols by measurement and modeling during CAREBeijing-2006, *Journal of*
836 *Geophysical Research-Atmospheres*, 114, 10.1029/2008jd010805, 2009.

837 Liu, Z., Wang, Y., Gu, D., Zhao, C., Huey, L. G., Stickel, R., Liao, J., Shao, M., Zhu,
838 T., Zeng, L., Amoroso, A., Costabile, F., Chang, C. C., and Liu, S. C.: Summertime
839 photochemistry during CAREBeijing-2007: ROx budgets and O-3 formation,
840 *Atmospheric Chemistry and Physics*, 12, 7737-7752, 10.5194/acp-12-7737-2012,
841 2012.

842 Lou, S. J., Liao, H., and Zhu, B.: Impacts of aerosols on surface-layer ozone
843 concentrations in China through heterogeneous reactions and changes in
844 photolysis rates, *Atmospheric Environment*, 85, 123-138,
845 10.1016/j.atmosenv.2013.12.004, 2014.

846 Lu, K., Fuchs, H., Hofzumahaus, A., Tan, Z., Wang, H., Zhang, L., Schmitt, S. H.,
847 Rohrer, F., Bohn, B., Broch, S., Dong, H., Gkatzelis, G. I., Hohaus, T., Holland, F.,
848 Li, X., Liu, Y., Liu, Y., Ma, X., Novelli, A., Schlag, P., Shao, M., Wu, Y., Wu, Z.,
849 Zeng, L., Hu, M., Kiendler-Scharr, A., Wahner, A., and Zhang, Y.: Fast
850 Photochemistry in Wintertime Haze: Consequences for Pollution Mitigation
851 Strategies, *Environmental Science & Technology*, 53, 10676-10684,
852 10.1021/acs.est.9b02422, 2019.

853 Lu, K. D., Hofzumahaus, A., Holland, F., Bohn, B., Brauers, T., Fuchs, H., Hu, M.,
854 Haseler, R., Kita, K., Kondo, Y., Li, X., Lou, S. R., Oebel, A., Shao, M., Zeng, L.
855 M., Wahner, A., Zhu, T., Zhang, Y. H., and Rohrer, F.: Missing OH source in a
856 suburban environment near Beijing: observed and modelled OH and HO₂
857 concentrations in summer 2006, *Atmospheric Chemistry and Physics*, 13, 1057-
858 1080, 10.5194/acp-13-1057-2013, 2013.

859 Lu, X., Hong, J., Zhang, L., Cooper, O. R., Schultz, M. G., Xu, X., Wang, T., Gao, M.,
860 Zhao, Y., and Zhang, Y.: Severe Surface Ozone Pollution in China: A Global
861 Perspective, *Environmental Science & Technology Letters*, 5, 487-494,
862 10.1021/acs.estlett.8b00366, 2018.

863 Ma, Z. Q., Xu, J., Quan, W. J., Zhang, Z. Y., Lin, W. L., and Xu, X. B.: Significant
864 increase of surface ozone at a rural site, north of eastern China, *Atmospheric*
865 *Chemistry and Physics*, 16, 3969-3977, 10.5194/acp-16-3969-2016, 2016a.

866 Ma, Z. W., Hu, X. F., Sayer, A. M., Levy, R., Zhang, Q., Xue, Y. G., Tong, S. L., Bi, J.,
867 Huang, L., and Liu, Y.: Satellite-Based Spatiotemporal Trends in PM_{2.5}
868 Concentrations: China, 2004-2013, *Environmental Health Perspectives*, 124, 184-
869 192, 10.1289/ehp.1409481, 2016b.

870 Madronich, S.: The atmosphere and UV-B radiation at ground level, in: *Environmental*
871 *UV photobiology*, Springer, 1-39, 1993.

872 Matthews, P. S. J., Baeza-Romero, M. T., Whalley, L. K., and Heard, D. E.: Uptake of
873 HO₂ radicals onto Arizona test dust particles using an aerosol flow
874 tube, *Atmos. Chem. Phys.*, 14, 7397-7408, 10.5194/acp-14-7397-2014, 2014.

875 Mihelcic, D., Holland, F., Hofzumahaus, A., Hoppe, L., Konrad, S., Musgen, P., Patz,
876 H. W., Schafer, H. J., Schmitz, T., Volz-Thomas, A., Bachmann, K., Schlomski, S.,
877 Platt, U., Geyer, A., Alicke, B., and Moortgat, G. K.: Peroxy radicals during
878 BERLIOZ at Pabstthum: Measurements, radical budgets and ozone production,
879 *Journal of Geophysical Research-Atmospheres*, 108, 17, 10.1029/2001jd001014,
880 2003.

881 Moghani, M., Archer, C. L., and Mirzakhali, A.: The importance of transport to ozone
882 pollution in the US Mid-Atlantic, *Atmos. Environ.*, 191, 420-431, 2018.

883 Monks, P. S., Archibald, A. T., Colette, A., Cooper, O., Coyle, M., Derwent, R., Fowler,
884 D., Granier, C., Law, K. S., Mills, G. E., Stevenson, D. S., Tarasova, O., Thouret,
885 V., von Schneidemesser, E., Sommariva, R., Wild, O., and Williams, M. L.:
886 Tropospheric ozone and its precursors from the urban to the global scale from air
887 quality to short-lived climate forcer, *Atmospheric Chemistry and Physics*, 15,
888 8889-8973, 10.5194/acp-15-8889-2015, 2015.

889 Ni, M. J., Huang, J. X., Lu, S. Y., Li, X. D., Yan, J. H., and Cen, K. F.: A review on
890 black carbon emissions, worldwide and in China, *Chemosphere*, 107, 83-93,
891 10.1016/j.chemosphere.2014.02.052, 2014.

892 Parrish, D. D., Xu, J., Croes, B., and Shao, M.: Air quality improvement in Los Angeles-
893 perspectives for developing cities, *Frontiers of Environmental Science &*
894 *Engineering*, 10, 10.1007/s11783-016-0859-5, 2016.

895 Peeters, J., Nguyen, T. L., and Vereecken, L.: HO_x radical regeneration in the oxidation
896 of isoprene, *Physical Chemistry Chemical Physics*, 11, 5935-5939,
897 10.1039/b908511d, 2009.

898 Pollack, I. B., Ryerson, T. B., Trainer, M., Neuman, J. A., Roberts, J. M., and Parrish,
899 D. D.: Trends in ozone, its precursors, and related secondary oxidation products in
900 Los Angeles, California: A synthesis of measurements from 1960 to 2010, *Journal*
901 *of Geophysical Research-Atmospheres*, 118, 5893-5911, 10.1002/jgrd.50472,
902 2013.

903 Qu, W. J., Wang, J., Zhang, X. Y., Wang, D., and Sheng, L. F.: Influence of relative
904 humidity on aerosol composition: Impacts on light extinction and visibility
905 impairment at two sites in coastal area of China, *Atmospheric Research*, 153, 500-
906 511, 10.1016/j.atmosres.2014.10.009, 2015.

907 Raga, G. B., Castro, T., and Baumgardner, D.: The impact of megacity pollution on
908 local climate and implications for the regional environment: Mexico City,
909 *Atmospheric Environment*, 35, 1805-1811, 10.1016/s1352-2310(00)00275-2,

910 2001.

911 Real, E., and Sartelet, K.: Modeling of photolysis rates over Europe: impact on
 912 chemical gaseous species and aerosols, *Atmos. Chem. Phys.*, 11, 1711-1727,
 913 10.5194/acp-11-1711-2011, 2011.

914 Shah, V., Jacob, D., Li, K., Silvern, R., Zhai, S., Liu, M., Lin, J., and Zhang, Q.: Effect
 915 of changing NO_x lifetime on the seasonality and long-term trends of satellite-
 916 observed tropospheric NO₂ columns over China, 2020.

917 Streets, D. G., Fu, J. S., Jang, C. J., Hao, J. M., and Yu, C.: Air quality during the 2008
 918 Beijing Olympic Games, *Atmospheric Environment (1967)*, 41, 4800-4492, 2007.

919 Taketani, F., Kanaya, Y., and Akimoto, H.: Kinetics of heterogeneous reactions of HO₂
 920 radical at ambient concentration levels with (NH₄)₂SO₄ and NaCl aerosol
 921 particles, *The Journal of Physical Chemistry A*, 112, 2370-2377, 2008.

922 Taketani, F., Kanaya, Y., Pochanart, P., Liu, Y., Li, J., Okuzawa, K., Kawamura, K.,
 923 Wang, Z., and Akimoto, H.: Measurement of overall uptake coefficients for HO₂
 924 radicals by aerosol particles sampled from ambient air at Mts. Tai and Mang
 925 (China), *Atmospheric Chemistry and Physics*, 12, 11907-11916, 10.5194/acp-12-
 926 11907-2012, 2012.

927 Tan, Z., Fuchs, H., Lu, K., Hofzumahaus, A., Bohn, B., Broch, S., Dong, H., Gomm, S.,
 928 Häsel, R., He, L., Holland, F., Li, X., Liu, Y., Lu, S., Rohrer, F., Shao, M., Wang,
 929 B., Wang, M., Wu, Y., Zeng, L., Zhang, Y., Wahner, A., and Zhang, Y.: Radical
 930 chemistry at a rural site (Wangdu) in the North China Plain: observation and model
 931 calculations of OH, HO₂ and RO₂ radicals, *Atmos. Chem. Phys.*, 17, 663-690,
 932 10.5194/acp-17-663-2017, 2017.

933 Tian, R., Ma, X., Jia, H., Yu, F., Sha, T., and Zan, Y.: Aerosol radiative effects on
 934 tropospheric photochemistry with GEOS-Chem simulations, *Atmospheric
 935 Environment*, 208, 82-94, 2019.

936 Verstraeten, W. W., Neu, J. L., Williams, J. E., Bowman, K. W., Worden, J. R., and
 937 Boersma, K. F.: Rapid increases in tropospheric ozone production and export from
 938 China, *Nature geoscience*, 8, 690, 2015.

939 Wang, B., Shao, M., Lu, S. H., Yuan, B., Zhao, Y., Wang, M., Zhang, S. Q., and Wu, D.:
 940 Variation of ambient non-methane hydrocarbons in Beijing city in summer 2008,
 941 *Atmospheric Chemistry and Physics*, 10, 5911-5923, 10.5194/acp-10-5911-2010,
 942 2010.

943 Wang, H., Lu, K., Tan, Z., Sun, K., Li, X., Hu, M., Shao, M., Zeng, L., Zhu, T., and
 944 Zhang, Y.: Model simulation of NO₃, N₂O₅ and ClNO₂ at a rural site in Beijing
 945 during CAREBeijing-2006, *Atmospheric Research*, 196, 97-107, 2017.

946 Wang, J., Allen, D. J., Pickering, K. E., Li, Z., and He, H.: Impact of aerosol direct
 947 effect on East Asian air quality during the EAST-AIRE campaign, *Journal of
 948 Geophysical Research: Atmospheres*, 121, 6534-6554, 2016a.

949 Wang, J. L., Din, G. Z., and Chan, C. C.: Validation of a laboratory-constructed
 950 automated gas chromatograph for the measurement of ozone precursors through
 951 comparison with a commercial analogy, *Journal of Chromatography A*, 1027, 11-
 952 18, 10.1016/j.chroma.2003.08.099, 2004.

953 Wang, M., Zeng, L., Lu, S., Shao, M., Liu, X., Yu, X., Chen, W., Yuan, B., Zhang, Q.,

954 Hu, M., and Zhang, Z.: Development and validation of a cryogen-free automatic
955 gas chromatograph system (GC-MS/FID) for online measurements of volatile
956 organic compounds, *Analytical Methods*, 6, 9424-9434, 10.1039/c4ay01855a,
957 2014.

958 Wang, M., Shao, M., Chen, W., Lu, S., Liu, Y., Yuan, B., Zhang, Q., Zhang, Q., Chang,
959 C. C., Wang, B., Zeng, L., Hu, M., Yang, Y., and Li, Y.: Trends of non-methane
960 hydrocarbons (NMHC) emissions in Beijing during 2002-2013, *Atmospheric
961 Chemistry and Physics*, 15, 1489-1502, 10.5194/acp-15-1489-2015, 2015a.

962 Wang, P., Wang, T., and Ying, Q.: Regional source apportionment of summertime ozone
963 and its precursors in the megacities of Beijing and Shanghai using a source-
964 oriented chemical transport model, *Atmos. Environ.*, 224, 10,
965 10.1016/j.atmosenv.2020.117337, 2020.

966 Wang, Q. Q., Sun, Y. L., Jiang, Q., Du, W., Sun, C. Z., Fu, P. Q., and Wang, Z. F.:
967 Chemical composition of aerosol particles and light extinction apportionment
968 before and during the heating season in Beijing, China, *Journal of Geophysical
969 Research-Atmospheres*, 120, 12708-12722, 10.1002/2015jd023871, 2015b.

970 Wang, W., Li, X., Shao, M., Hu, M., Zeng, L., Wu, Y., and Tan, T.: The impact of
971 aerosols on photolysis frequencies and ozone production in Beijing during the 4-
972 year period 2012–2015, *Atmos. Chem. Phys.*, 19, 9413-9429, 10.5194/acp-19-
973 9413-2019, 2019.

974 Wang, X. M., Chen, W. H., Chen, D. H., Wu, Z. Y., and Fan, Q.: Long-term trends of
975 fine particulate matter and chemical composition in the Pearl River Delta
976 Economic Zone (PRDEZ), China, *Front. Env. Sci. Eng.*, 10, 53-62,
977 10.1007/s11783-014-0728-z, 2016b.

978 Wang, Y., Zhang, Y., Hao, J., and Luo, M.: Seasonal and spatial variability of surface
979 ozone over China: contributions from background and domestic pollution,
980 *Atmospheric Chemistry and Physics*, 11, 3511-3525, 10.5194/acp-11-3511-2011,
981 2011.

982 Warneke, C., de Gouw, J. A., Holloway, J. S., Peischl, J., Ryerson, T. B., Atlas, E., Blake,
983 D., Trainer, M., and Parrish, D. D.: Multiyear trends in volatile organic compounds
984 in Los Angeles, California: Five decades of decreasing emissions, *Journal of
985 Geophysical Research-Atmospheres*, 117, 10.1029/2012jd017899, 2012.

986 Wehner, B., Birmili, W., Ditas, F., Wu, Z., Hu, M., Liu, X., Mao, J., Sugimoto, N., and
987 Wiedensohler, A.: Relationships between submicrometer particulate air pollution
988 and air mass history in Beijing, China, 2004-2006, *Atmospheric Chemistry and
989 Physics*, 8, 6155-6168, 10.5194/acp-8-6155-2008, 2008.

990 Wendisch, M., Mertes, S., Ruggaber, A., and Nakajima, T.: Vertical profiles of aerosol
991 and radiation and the influence of a temperature inversion: Measurements and
992 radiative transfer calculations, *J. Appl. Meteorol.*, 35, 1703-1715, 10.1175/1520-
993 0450(1996)035<1703:vpoaar>2.0.co;2, 1996.

994 Xie, X., Shao, M., Liu, Y., Lu, S., Chang, C.-C., and Chen, Z.-M.: Estimate of initial
995 isoprene contribution to ozone formation potential in Beijing, China, *Atmospheric
996 Environment*, 42, 6000-6010, 10.1016/j.atmosenv.2008.03.035, 2008.

997 Xing, J., Wang, J., Mathur, R., Wang, S., Sarwar, G., Pleim, J., Hogrefe, C., Zhang, Y.,

998 Jiang, J., and Wong, D. C.: Impacts of aerosol direct effects on tropospheric ozone
999 through changes in atmospheric dynamics and photolysis rates, *Atmospheric*
1000 *chemistry and physics*, 17, 9869, 2017.

1001 Xu, J., Ma, J. Z., Zhang, X. L., Xu, X. B., Xu, X. F., Lin, W. L., Wang, Y., Meng, W.,
1002 and Ma, Z. Q.: Measurements of ozone and its precursors in Beijing during
1003 summertime: impact of urban plumes on ozone pollution in downwind rural areas,
1004 *Atmospheric Chemistry and Physics*, 11, 12241-12252, 10.5194/acp-11-12241-
1005 2011, 2011.

1006 Xu, J., Zhang, Y. H., Zheng, S. Q., and He, Y. J.: Aerosol effects on ozone
1007 concentrations in Beijing: A model sensitivity study, *J. Environ. Sci.*, 24, 645-656,
1008 10.1016/s1001-0742(11)60811-5, 2012.

1009 Yuan, B., Shao, M., de Gouw, J., Parrish, D. D., Lu, S., Wang, M., Zeng, L., Zhang, Q.,
1010 Song, Y., Zhang, J., and Hu, M.: Volatile organic compounds (VOCs) in urban air:
1011 How chemistry affects the interpretation of positive matrix factorization (PMF)
1012 analysis, *Journal of Geophysical Research-Atmospheres*, 117,
1013 10.1029/2012jd018236, 2012.

1014 Zhang, J. P., Zhu, T., Zhang, Q. H., Li, C. C., Shu, H. L., Ying, Y., Dai, Z. P., Wang, X.,
1015 Liu, X. Y., Liang, A. M., Shen, H. X., and Yi, B. Q.: The impact of circulation
1016 patterns on regional transport pathways and air quality over Beijing and its
1017 surroundings, *Atmospheric Chemistry and Physics*, 12, 5031-5053, 10.5194/acp-
1018 12-5031-2012, 2012.

1019 Zhang, L., Shao, J. Y., Lu, X., Zhao, Y. H., Hu, Y. Y., Henze, D. K., Liao, H., Gong, S.
1020 L., and Zhang, Q.: Sources and Processes Affecting Fine Particulate Matter
1021 Pollution over North China: An Adjoint Analysis of the Beijing APEC Period,
1022 *Environ. Sci. Technol.*, 50, 8731-8740, 10.1021/acs.est.6b03010, 2016.

1023 Zhang, Q., Yuan, B., Shao, M., Wang, X., Lu, S., Lu, K., Wang, M., Chen, L., Chang,
1024 C. C., and Liu, S. C.: Variations of ground-level O₃ and its precursors in Beijing
1025 in summertime between 2005 and 2011, *Atmospheric Chemistry and Physics*, 14,
1026 6089-6101, 10.5194/acp-14-6089-2014, 2014.

1027 Zhao, B., Wang, S. X., Liu, H., Xu, J. Y., Fu, K., Klimont, Z., Hao, J. M., He, K. B.,
1028 Cofala, J., and Amann, M.: NO_x emissions in China: historical trends and future
1029 perspectives, *Atmospheric Chemistry and Physics*, 13, 9869-9897, 10.5194/acp-
1030 13-9869-2013, 2013.

1031 Zhao, P. S., Zhang, X. L., and Xu, X. F.: Long-term visibility trends and characteristics
1032 in the region of Beijing, Tianjin, and Hebei, China, *Abstr. Pap. Am. Chem. Soc.*,
1033 242, 1, 2011.

1034 Zheng, C., Zhao, C., Zhu, Y., Wang, Y., Shi, X., Wu, X., Chen, T., Wu, F., and Qiu, Y.:
1035 Analysis of influential factors for the relationship between PM_{2.5} and AOD in
1036 Beijing, *Atmospheric Chemistry and Physics*, 17, 13473-13489, 2017.

1037 Zou, Q., Song, H., Tang, M., and Lu, K.: Measurements of HO₂ uptake coefficient on
1038 aqueous (NH₄)₂SO₄ aerosol using aerosol flow tube with LIF system, *Chin.*
1039 *Chem. Lett.*, 30, 2236-2240, <https://doi.org/10.1016/j.cclet.2019.07.041>, 2019.

1040